

Slice Monte Carlo Integration

Johannes K. Krondorfer,¹ Christian W. Binder,² Matthias Neumann,^{3,4} and Wolfgang von der Linden^{4,5}

¹*Institute of Experimental Physics, Graz University of Technology, Petersgasse 16, 8010 Graz, Austria*

²*Department of Physics, University of Oxford, Parks Rd, Oxford OX1 3PJ, United Kingdom*

³*Institute of Statistics, Graz University of Technology, Kopernikusgasse 24/III, 8010 Graz, Austria*

⁴*GraML – Graz Center for Machine Learning, Rechbauerstraße 12, 8010, Graz, Austria*

⁵*Institute of Theoretical and Computational Physics, Graz University of Technology, Petersgasse 16, 8010 Graz, Austria*

(Dated: June 9, 2026)

Numerical integration involving expensive target functions is a common bottleneck in Bayesian inference and simulation. When a cheap surrogate is available, standard approaches such as reweighting or importance sampling often suffer from high variance and inefficient use of function evaluations. We introduce Slice Monte Carlo integration ($S\ell$ MC), a method that leverages a Nested Sampling-like procedure on the surrogate to partition the space into informative strata, or *slices*, while generating samples in the parameter space drawn from the prior within each slice. This enables stratified Monte Carlo integration of the expensive target function over the surrogate-induced partition, yielding an efficient estimate of the target integral. A key advantage of $S\ell$ MC is the decoupling of slice volume estimation from target function evaluation, which allows for adaptive, variance-aware allocation of computational effort. We investigate the properties of $S\ell$ MC, demonstrate how to efficiently generate posterior samples, and validate the method on simple benchmark problems.

Keywords: nested sampling, importance sampling, stratified Monte Carlo sampling, evidence calculation, posterior samples, surrogate models, reweighting, partition function

I. INTRODUCTION

Efficient numerical integration is a key challenge in many disciplines, including data science, physics, engineering, and Bayesian statistics, where high-dimensional integrals arise in tasks such as model selection^{1,2}, parameter estimation and uncertainty quantification³⁻⁸, and partition function evaluation⁹⁻¹³. While classical quadrature methods quickly become intractable in high dimensions, stochastic methods such as Monte Carlo integration, importance sampling¹⁴⁻¹⁷, and Nested Sampling^{18,19} have proven effective when the integrand is inexpensive to evaluate.

In many scientific and engineering applications, however, evaluating the target function is computationally expensive. A single evaluation may require a large-scale simulation, the solution of a complex physical model, or the processing of high-resolution data^{5,7,10}. In such settings, standard integration methods can become inefficient because they require many target evaluations. At the same time, low-fidelity approximations or surrogate models are often available and capture useful structure of the integrand at substantially lower cost. These approximations may take the form of coarse physical models^{7,8}, simplified energy landscapes^{10,12}, or machine-learned regressors trained on high-fidelity data²⁰⁻²⁴. The central challenge is to use such approximations to guide integration, accelerate computation, and reduce variance without introducing bias.

Several approaches have been proposed to address this challenge. Sequential Monte Carlo methods construct a sequence of weighted particle approximations to the target distribution, often combining reweighting, resampling, and mutation steps to balance bias and variance^{25,26}. Multifidelity Monte Carlo and Multilevel Monte Carlo methods combine simulations at different fidelities using control variates or telescoping estimators to reduce variance while maintaining unbiasedness²⁷⁻²⁹. Adaptive importance sampling techniques construct proposal distributions informed by surrogate models or auxiliary densities to concentrate samples in high-contribution regions^{14,30}. Stratified sampling methods reduce variance by partitioning the parameter space into regions of approximately equal weight. However, standard stratification often relies on simple strata, such as axis-aligned partitions¹⁵, which may poorly reflect complex posterior geometries. While these methods can perform well for expectation estimation, they often struggle to scale efficiently to high-dimensional or multimodal distributions, and typically do not yield posterior samples without additional approximation or resampling techniques^{31,32}.

In contrast, Nested Sampling provides a framework for estimating Bayesian evidence and generating posterior samples simultaneously^{18,19}. By constructing nested likelihood contours and estimating the associated constrained prior masses, it enables efficient exploration of complicated multimodal distributions. Recent extensions incorporate dynamic allocation of samples^{33,34}, slice-sampling-based exploration of the

constrained prior in high dimensions³⁵, or adaptations for multimodality^{32,36,37}, but they still rely on target evaluations to estimate constrained prior masses. Moreover, reweighting schemes based on Nested Sampling still require many target evaluations, because the fidelity of the volume estimate remains directly tied to the number of target function calls, as we discuss in Section II C.

In this paper, we introduce Slice Monte Carlo integration ($S\ell MC$), a method that combines the strengths of stratified Monte Carlo and Nested Sampling for surrogate-based integration. $S\ell MC$ applies a Nested Sampling-like procedure to the surrogate to partition the space into informative strata, or *slices*, while generating prior samples within each slice. This enables stratified Monte Carlo integration over the surrogate-induced partition and yields efficient estimates of the target integral. A key advantage over standard reweighting techniques is that volume estimation is decoupled from target function evaluation. Slice volumes can therefore be estimated accurately using the cheap surrogate, while expensive target evaluations are allocated adaptively across slices. Furthermore, the surrogate-induced partition facilitates efficient generation of posterior samples via rejection sampling.

The term slice in this paper denotes surrogate-induced strata for integration. This differs from Neal’s slice sampling for Markov chain Monte Carlo³⁸, and from the use of slice sampling as a constrained-prior sampler in NS implementations such as PolyChord³⁵.

The remainder of this paper is structured as follows. In Section II, we formalize the problem setup and review stochastic integration methods relevant to the development of $S\ell MC$. Section III introduces the slicing framework, followed by a detailed presentation of the $S\ell MC$ algorithm, including its theoretical properties, such as unbiasedness and variance, and a discussion on generating posterior samples. Finally, Section IV demonstrates the performance of the proposed method on benchmark problems.

II. PROBLEM SETUP AND RELATED METHODS

We are interested in evaluating integrals of the form

$$\mathcal{Z} = \mathbb{E}_{\pi}[L] = \int_{\Omega} L(\theta) \, d\pi(\theta), \quad (1)$$

over a Borel-measurable parameter space $\Omega \subset \mathbb{R}^d$ for $d \geq 1$, where $L : \Omega \rightarrow \mathbb{R}$ is the target function and π is a prior probability distribution on Ω . Specifically, this includes evidence integrals in the context of Bayesian inference, where L is the non-negative likelihood function or partition function in statistical physics, e.g., the non-negative exponential Boltzmann factor. This integral is particularly demanding

because the prior probability distribution function $\pi(\theta)$ typically has a much smaller variability than the target function $L(\theta)$.

Another goal of this paper is based on the posterior distribution $dp(\theta) = L(\theta) d\pi(\theta) / \mathcal{Z}$, for which either the generation of uncorrelated samples or posterior expectation values of the form

$$\mathcal{G} = \mathbb{E}_p[g] = \int_{\Omega} g(\theta) dp(\theta). \quad (2)$$

are of great interest. This type of problem arises in many contexts, including statistical inference, uncertainty quantification, and statistical physics, where, e.g., the posterior expectation corresponds to the thermodynamic expectation of some physical observable.

To estimate such integrals and obtain samples, various stochastic integration techniques have been developed. Below, we briefly review the most relevant integration approaches that form the conceptual foundation for Slice Monte Carlo integration (S ℓ MC) proposed in the present paper.

A. Monte Carlo Integration

In standard Monte Carlo integration (simple sampling), expectations with respect to π are estimated using the empirical mean over independent and identically distributed samples $\Theta_1, \dots, \Theta_N \stackrel{\text{iid}}{\sim} \pi$. For the evidence integral $\mathcal{Z} = \mathbb{E}_{\pi}[L]$, this yields the estimator

$$\hat{\mathcal{Z}}_N^{\text{MC}} = \frac{1}{N} \sum_{i=1}^N L(\Theta_i), \quad (3)$$

which is unbiased, converges at rate $\mathcal{O}(N^{-1/2})$ and is asymptotically normal provided that $\text{Var}_{\pi}[L] < \infty$.¹⁶ Its variance is given by

$$\text{Var}[\hat{\mathcal{Z}}_N^{\text{MC}}] = \frac{1}{N} \text{Var}_{\pi}[L]. \quad (4)$$

1. Monte Carlo Importance Sampling

Simple sampling may be inefficient when significant contributions to \mathcal{Z} come from regions of low probability under π . If a nonnegative surrogate function $\phi(\theta)$ can be found for which the integral $\mathcal{Z}_{\phi} = \mathbb{E}_{\pi}[\phi]$ is known, or can easily be evaluated to arbitrary precision, then one can introduce a new probability measure $dp_{\phi}(\theta) = \phi(\theta) d\pi(\theta) / \mathcal{Z}_{\phi}$ and the target integral \mathcal{Z} can be written as

$$\mathcal{Z} = \mathcal{Z}_{\phi} \mathbb{E}_{p_{\phi}}[L/\phi]. \quad (5)$$

The resulting Monte Carlo estimator, which we refer to as importance sampling (IS) estimator, remains unbiased and has variance

$$\text{Var}[\widehat{\mathcal{Z}}_N^{\text{IS}}] = \frac{\mathcal{Z}_\phi^2}{N} \text{Var}_{p_\phi}[L/\phi]. \quad (6)$$

Crucially, \mathcal{Z}_ϕ must be known, which in itself can be a complicated task. If the surrogate $\phi(\theta)$ resembles closely the target function $L(\theta)$ then the numerical effort to compute \mathcal{Z}_ϕ is the same as the numerical effort to compute \mathcal{Z} , unless it allows an analytical evaluation, or to use more efficient numerical techniques which are not applicable to $L(\theta)$. Moreover, the choice of ϕ strongly influences efficiency. A mismatch between ϕ and L can lead to a large variance of the estimator. Adaptive schemes that iteratively construct surrogates, e.g. product approximations $\phi(\theta) = \prod_{j=1}^d g_j(\theta_j)$, have been proposed^{14,17}, but typically rely on independence assumptions across dimensions.

2. Stratified Monte Carlo Integration

Stratification can also reduce the variance of the integrand. To that purpose, Ω is partitioned into disjoint regions (strata) $\mathcal{S}_1, \dots, \mathcal{S}_M$, with $\Omega = \cup_{i=1}^M \mathcal{S}_i$, and the integral can be written as

$$\mathcal{Z} = \sum_{i=1}^M \int_{\mathcal{S}_i} L(\theta) \, d\pi(\theta). \quad (7)$$

Each term is then estimated separately via Monte Carlo

$$\widehat{\mathcal{Z}}_{\mathcal{S}} = \sum_{i=1}^M \frac{S_i}{N_i} \sum_{k=1}^{N_i} L(\Theta_{i,k}), \quad (8)$$

where $S_i = \pi[\mathcal{S}_i]$ is the prior mass of stratum \mathcal{S}_i , and $\Theta_{i,k} \stackrel{iid}{\sim} \pi|_{\mathcal{S}_i}$ for $i = 1, \dots, M$ and $k = 1, \dots, N_i$.

Sample allocation can be optimized to minimize the total variance. Writing $N = \sum_{i=1}^M N_i$, the optimal allocation is¹⁵

$$\frac{N_i}{N} = \frac{S_i \sigma_{\mathcal{S}_i}}{\sum_{k=1}^M S_k \sigma_{\mathcal{S}_k}}, \quad (9)$$

where $\sigma_{\mathcal{S}_i}^2 = \text{Var}_{\pi}[L(\Theta)|\Theta \in \mathcal{S}_i]$ denotes the variance of L in stratum \mathcal{S}_i . So the minimal variance, if only the number of points per stratum N_1, \dots, N_M are optimized, reads

$$\text{Var}_{\text{opt}}[\widehat{\mathcal{Z}}_{\mathcal{S}}] = \frac{1}{N} \left(\sum_{i=1}^M S_i \sigma_{\mathcal{S}_i} \right)^2 \quad (10)$$

as compared to

$$\text{Var}_{\text{eq}}[\widehat{\mathcal{Z}}_{\mathcal{J}}] = \frac{M}{N} \sum_{i=1}^M S_i^2 \sigma_{\mathcal{J}_i}^2 \quad (11)$$

if the same number $N_i = N/M$ is used in all strata. The difference

$$\text{Var}_{\text{eq}}[\widehat{\mathcal{Z}}_{\mathcal{J}}] - \text{Var}_{\text{opt}}[\widehat{\mathcal{Z}}_{\mathcal{J}}] = \frac{M}{N} \left(\sum_{i=1}^M [S_i \sigma_{\mathcal{J}_i} - \overline{S\sigma}]^2 \right) > 0, \quad \text{with } \overline{S\sigma} := \frac{1}{M} \sum_{i=1}^M S_i \sigma_{\mathcal{J}_i} \quad (12)$$

Despite its potential, stratification poses two key challenges: identifying effective strata *a priori* is nontrivial in high dimensions, and sampling from the prior within each stratum may be difficult and computationally expensive. Common approaches use axis-aligned partitions or recursive bisection along directions of high variance^{15,17}. Adaptive stratification can improve performance, but a large number of evaluations may still be needed. Additionally, simple bisections of dimensions can violate symmetries of the integrand and therefore reduce the efficiency. This limitation is addressed in *SℓMC*, where we design informative strata that are adapted to the target function, via a Nested Sampling-like procedure applied to a surrogate.

B. Nested Sampling

1. Rewriting the Evidence Integral

Before introducing *SℓMC*, we briefly review the principles of Nested Sampling (NS). NS begins by reformulating the evidence integral in Equation (1) over a positive likelihood function $L : \Omega \rightarrow \mathbb{R}_{>0}$ as an integral over the constrained prior mass $X(\lambda) := \pi[L(\Theta) > \lambda]$

$$\mathcal{Z} = \int_0^1 \widetilde{L}(x) \, dx, \quad (13)$$

where

$$\widetilde{L}(x) = \sup\{\lambda \in \mathbb{R} \mid X(\lambda) > x\} \quad (14)$$

is the generalized inverse of X , also interpreted as the likelihood corresponding to the contour enclosing prior mass x ^{18,19,39–41}.

This transforms the high-dimensional integral into a one-dimensional integral over the unit interval, which can then be approximated using standard quadrature

$$\mathcal{Z} \approx Z = \sum_{i=1}^K w_i \widetilde{L}_i, \quad (15)$$

where $w_i = X_{i-1} - X_i$ are weights associated with prior mass differences and \tilde{L}_i are corresponding likelihood values.

Since $\tilde{L}(x)$ is a monotonically decreasing function in the constrained prior mass x , Equation (15) yields an upper bound for the true \mathcal{Z} , while $\sum_{i=1}^K w_i \tilde{L}_{i-1}$ is a strict lower bound. However, evaluating $X(\lambda)$ exactly is intractable, and it must be approximated stochastically.^{18,19}

2. The Nested Sampling Procedure

NS estimates X by random sampling from level sets of increasing likelihood. The key identity is that for $\Theta \sim \pi|_{>L^*}$, i.e. drawn from the prior constrained to the set $\{L > L^*\}$, $X(L(\Theta)) \sim \text{Uniform}(0, X^*)$, where $X^* = X(L^*)$. This identity holds if X is continuous, which is the case if L has no plateaus of non-zero probability with respect to π .^{40,41}

By drawing N_{live} independent samples from $\pi|_{>L^*}$ and sorting them by likelihood,

$$\begin{aligned} L_{(1)} &> L_{(2)} > \dots > L_{(N_{\text{live}})} \\ X_{(1)} &< X_{(2)} < \dots < X_{(N_{\text{live}})}, \end{aligned} \quad (16)$$

the smallest likelihood corresponds to a prior mass $X_{(N_{\text{live}})} = tX^*$ where $t \sim \text{Beta}(N_{\text{live}}, 1)$, as given by the maximum statistics.^{19,39} The number N_{live} is typically referred to as the number of live points.

This procedure can be used to compress the prior mass iteratively, via the recursion

$$X_i = t_i X_{i-1}, \quad \text{with } t_i \sim \text{Beta}(N_{\text{live}}, 1), \quad X_0 = 1, \quad (17)$$

The contraction factors t_i are mutually independent, as they are associated with independent uniform samples from the constrained prior. Conditional on the sampled likelihood values $\{\tilde{L}_i\}$, the quadrature estimate is therefore a function of the compression factors, and we write $Z = Z(\mathbf{t})$ to indicate this dependence, where $\mathbf{t} = (t_1, \dots, t_K)$ denotes the vector of compression factors.

At each step, the live point with the lowest likelihood is discarded and stored, and a new point is drawn from the new constrained prior $\pi|_{>L_i}$. In practice the constrained draw is the dominant cost of NS, and a variety of constrained samplers have been proposed, ranging from standard Markov chain Monte Carlo methods¹⁹ and ellipsoidal rejection³² to slice-sampling chains³⁵. The other live points already fulfill the constraint by construction. Repeating this for K steps yields a sequence $\{\theta_i, \tilde{L}_i, X_i(\mathbf{t})\}$ which forms the quadrature rule in Equation (15). The use of the maximum statistic in each iteration is optimal in nested sampling, as it minimizes the estimator variance and maximizes the resolution of the quadrature.¹⁹ While alternative order statistics are theoretically possible, they generally lead to inferior performance. To ensure

that the quadrature adequately captures the bulk of the posterior mass, the number of iterations should satisfy $K \geq N_{\text{live}}H$, where H is the relative entropy (or Kullback–Leibler divergence) from the posterior to the prior.¹⁹ This condition ensures that the nested sampling trajectory penetrates deeply enough into high-likelihood regions to estimate both the evidence and the posterior accurately.

Dynamic nested sampling methods^{33,34} extend this framework by adaptively varying the number of points and termination criteria during sampling to enhance efficiency, particularly in the estimation of posterior expectations.

3. Error analysis

NS in this form produces not only a point estimate but a distribution over evidence estimates $Z(\mathbf{t})$, conditional on the sampled likelihood values, which we indicate by conditioning on $\boldsymbol{\theta}$. The remaining uncertainty in $Z(\mathbf{t})$ then comes from the stochastic compression factors \mathbf{t} . The compression factors may be set deterministically, e.g., $t_i = \exp(-1/N_{\text{live}})$ or $t_i = N_{\text{live}}/(N_{\text{live}} + 1)$, or sampled from $\text{Beta}(N_{\text{live}}, 1)$.^{19,39,42–44}

From now on, we assume that t_1, \dots, t_K are iid with $t_1 \sim \text{Beta}(N_{\text{live}}, 1)$. Error analysis can be conducted either using information-theoretic arguments¹⁹, or through a moment-based analysis^{39,42}. The latter approach yields formulas for the expectation and variance of $Z(\mathbf{t})$, given the knowledge of all sampled points during the procedure. Exploiting the independence of the compression factors t_i and using $\mathbb{E}[t_i] = N_{\text{live}}/(N_{\text{live}} + 1)$, one obtains

$$\mathbb{E}[Z|\boldsymbol{\theta}] = \sum_{i=1}^K \mathbb{E}[w_i|\boldsymbol{\theta}] \tilde{L}_i = \frac{1}{N_{\text{live}}} \sum_{i=1}^K \left(\frac{N_{\text{live}}}{N_{\text{live}} + 1} \right)^i \tilde{L}_i. \quad (18)$$

In practical applications, it is often sufficient to consider the distribution $Z(\mathbf{t})$ given the observed data, whose uncertainty arises from the stochastic nature of NS. Taking its conditional expectation yields a Bayesian point estimator of the evidence. It can be shown that this point estimator is asymptotically unbiased and asymptotically normally distributed under additional regularity conditions.⁴⁵ Note, however, that the remaining randomness of the point estimator is contained in \tilde{L}_i , which are obtained by the sorting procedure, and therefore, a simple error analysis of the point estimator is not applicable. Nevertheless, reformulations in terms of sequential Monte Carlo algorithms exist, which provide an inherently unbiased estimator for Nested Sampling.²⁵ For high-dimensional integrals, Skilling pointed out that instead of Z the relevant quantity is $\log(Z)$, which is usually closer to a normal distribution.^{39,46}

For the conditional variance,^{39,42} provide an explicit expression when the number of live points is constant. Here we will only investigate the general structure of the

variance, to analyze the sources of uncertainty,

$$\text{Var}[Z|\boldsymbol{\theta}] = \text{Var}\left[\sum_{i=1}^K w_i \tilde{L}_i | \boldsymbol{\theta}\right] = \sum_{i=1}^K \tilde{L}_i^2 \text{Var}[w_i | \boldsymbol{\theta}] + 2 \sum_{\substack{i,j=1 \\ i < j}}^K \tilde{L}_i \tilde{L}_j \text{Cov}[w_i, w_j | \boldsymbol{\theta}]. \quad (19)$$

Using the decomposition $w_j = X_i \prod_{k=i+1}^{j-1} t_k (1 - t_j)$ and the independence of the compression factors, we get

$$\text{Var}[Z|\boldsymbol{\theta}] = \sum_{i=1}^K \left(\tilde{L}_i^2 \text{Var}[w_i | \boldsymbol{\theta}] + 2 \tilde{L}_i \text{Cov}[w_i, X_i | \boldsymbol{\theta}] \sum_{j=i+1}^K \left(\tilde{L}_j \mathbb{E}[1 - t_j] \prod_{k=i+1}^{j-1} \mathbb{E}[t_k] \right) \right). \quad (20)$$

We will see in Section III B, why this particular decomposition of the variance of NS allows for an easy interpretation of the variance terms present in SℓMC. Further details can also be found in³⁹, where it is also shown that for a large number of live points N_{live} , the variance of Z is $\mathcal{O}(1/N_{\text{live}})$ like in standard MC. This implies that increasing the number of live points reduces the uncertainty, but at a price: The mean compression factor for large N_{live} is $t \approx e^{-1/N_{\text{live}}}$, hence the mean prior mass at step i is $X_i \approx e^{-i/N_{\text{live}}}$. In realistic problems, the dominant part of the likelihood corresponds to a very small prior mass X^* , which has to be reached for convergence. The number of necessary steps m^* follows from $X_{m^*} = X^*$ and gives $m^* = N_{\text{live}} |\ln(X^*)|$. Hence, the number of steps and therefore the number of function evaluations increases proportionally to N_{live} and in turn inversely proportional to ε_Z^2 , the desired relative uncertainty. We see, the stochastic uncertainty in NS comes entirely from the constrained prior masses, which are determined by N_{live} . We will see later that it is possible to determine the thresholds differently and obtain a way to strongly reduce the uncertainty of the constrained prior masses by adding uncertainty to the likelihood values, which allows for more flexibility to optimize the algorithm.

4. Posterior Representatives

NS can also be used to generate posterior representatives. Since the weighted likelihood values \tilde{L}_i are associated with constrained prior masses X_i , one can assign normalized weights

$$p_i(\mathbf{t}) = w_i(\mathbf{t}) \tilde{L}_i / Z(\mathbf{t}) \quad (21)$$

to obtain a discrete approximation of the posterior distribution $dp(\boldsymbol{\theta}) = L(\boldsymbol{\theta}) d\pi(\boldsymbol{\theta}) / \mathcal{Z}$. This still contains the uncertainty of the compression factors \mathbf{t} . The probability \hat{p}_i for θ_i is now given by the mean $\mathbb{E}_{\mathbf{t}}[w_i(\mathbf{t}) \tilde{L}_i / Z(\mathbf{t})]$, which is easily obtained by MC

means. This can be used to estimate the expectation $\mathcal{G} := \mathbb{E}_p[g]$ of an p -integrable quantity $g : \Omega \rightarrow \mathbb{R}$ by

$$G(\mathbf{t}) = \sum_{i=1}^K p_i(\mathbf{t})g(\theta_i) \quad (22)$$

or to obtain an equally weighted posterior sample by accepting each θ_i with probability \hat{p}_i/C , with $C \geq \max_i \hat{p}_i$.¹⁹

Similarly, a sampling-based or moment-based error analysis is also possible in this case. However, it is unclear whether $g(\theta_i)$ is indeed a good representative of the function g within the volume associated with the weight w_i .⁴⁴

C. Reweighting

Similar to importance sampling, the NS procedure can be reused to estimate the integral of a target function L using a surrogate model ϕ .^{45,47,48} Specifically, if samples θ_i^ϕ are drawn using NS applied to ϕ , we can express the evidence Z for L as the expectation in Equation (5), yielding

$$Z(\mathbf{t}_\phi) = \sum_{i=1}^K p_{\phi,i}(\mathbf{t}_\phi) Z_\phi(\mathbf{t}_\phi) L(\theta_{\phi,i}) / \tilde{\phi}_i = \sum_{i=1}^K w_{\phi,i}(\mathbf{t}_\phi) L(\theta_{\phi,i}), \quad (23)$$

where $p_{\phi,i} = w_{\phi,i}\tilde{\phi}_i/Z_\phi$ are posterior representatives of the surrogate model, and $w_{\phi,i}$ the volume elements derived from the surrogate model. As a matter of fact, $w_{\phi,i}(\mathbf{t}_\phi)$ is independent of the likelihood and it therefore has the same PDF as $w_i(\mathbf{t})$. The estimator in Equation (23) is analogous to that of standard NS for Z , but here L is evaluated at the sampled points $\theta_{\phi,i}$ obtained by NS based on ϕ .

The surrogate-based quadrature inherits the volume uncertainty of NS applied to ϕ . In addition, if ϕ and L do not induce the same ordering, the value $L(\theta_{\phi,i})$ may be a poor representative of the target function over the prior-mass element $w_{\phi,i}$, which introduces an additional source of variance.

At first glance, Equation (23) looks like there is nothing gained by using the surrogate. One important advantage, however, is the fact that the generation of constrained prior points, which typically necessitates several likelihood evaluations^{19,35}, is done with the low-cost surrogate. And that is, as we will see in the results section, a huge advantage if the true likelihood is expensive.

A key advantage of reweighting over classical importance sampling is that it becomes NS when L and ϕ induce the same ordering over Ω , i.e. if $L(\theta_1) < L(\theta_2)$ is equivalent to $\phi(\theta_1) < \phi(\theta_2)$ for all $\theta_1, \theta_2 \in \Omega$. In this case, the nested samples $\theta_{\phi,i}$ and associated volumes $w_{\phi,i}$ exactly match those that would have been produced by applying NS directly to L , and the reweighted estimator reproduces the NS result.

As in standard NS, the stochasticity lies in the volume elements $w_{\phi,i}$, so moment-based error analysis⁴² still applies. However, a new source of error arises, as L may vary significantly within the region associated with $w_{\phi,i}$, making $L(\theta_{\phi,i})$ a potentially poor representative of that volume. Additionally, the number of point evaluations of L must match the number of estimated volumes $w_{\phi,i}$, tying computational cost to quadrature resolution. Both issues are directly addressed by $S\ell MC$, which decouples volume estimation from point evaluations for the target function and allows for adaptive sampling within each *slice*.

III. SLICING AND SLICE MONTE CARLO

A. Slicing – Partitioning of the Parameter Space

With these prerequisites in place, we now introduce the partitioning of the parameter space into slices and the corresponding slice Monte Carlo integration ($S\ell MC$), which combines ideas of Nested Sampling, reweighting, and stratified Monte Carlo. By using a positive function $\phi : \Omega \rightarrow \mathbb{R}_{>0}$, which can be chosen as a cheap surrogate for the target function L , the core idea is to construct a sequence of thresholds $\{\phi_i\}_{i=0}^{M-1}$, with $\phi_0 = 0$, using a Nested Sampling-like procedure. These thresholds define level sets

$$\mathcal{X}_i := \{\theta \in \Omega \mid \phi(\theta) > \phi_i\}, \quad X_i := \pi[\mathcal{X}_i], \quad i = 0, \dots, M-1. \quad (24)$$

where X_i is the constrained prior mass above ϕ_i . For notational convenience, we set $\mathcal{X}_M = \emptyset$ and $X_M = 0$. This induces a partition of the parameter space into slices

$$(\mathcal{S}_i, S_i) = (\mathcal{X}_{i-1} \setminus \mathcal{X}_i, X_{i-1} - X_i), \quad i = 1, \dots, M, \quad (25)$$

where $S_i = \pi[\mathcal{S}_i]$ is the prior mass in slice \mathcal{S}_i . After constructing the slices, we can use samples drawn from the constrained prior within each slice \mathcal{S}_i to compute the target integral *via* stratified Monte Carlo integration.

Constrained sampling within each slice is generally very demanding, due to two constraints – upper and lower – on the value of the slicing function ϕ . However, the Nested Sampling-like procedure, where only the lower constraint is used to construct the slices, can also be used to generate the necessary samples.

In each iteration $i = 1, \dots, M-1$ a new threshold $\phi_i > \phi_{i-1}$ is chosen. It may be chosen arbitrarily, prescribed in advance, informed by previous runs, or determined by choosing the k -th order statistic of an iid sample $\Theta \sim \pi|_{\mathcal{X}_{i-1}}$ above the current threshold ϕ_{i-1} . After the threshold is selected, N_i independent iid samples are drawn from the constrained prior

$$\Theta_{i-1,1}^{\mathcal{X}}, \dots, \Theta_{i-1,N_i}^{\mathcal{X}} \stackrel{\text{iid}}{\sim} \pi|_{\mathcal{X}_{i-1}}. \quad (26)$$

Then the number $\hat{n}_i^{\mathcal{X}}$ of points satisfying $\phi(\Theta) > \phi_i$, i.e.

$$\hat{n}_i^{\mathcal{X}} := \sum_{k=1}^{N_i} \mathbb{1}_{\mathcal{X}_i}(\Theta_{i-1,k}^{\mathcal{X}}), \quad (27)$$

where $\mathbb{1}$ denotes the set indicator function, is binomial, $\hat{n}_i^{\mathcal{X}} \sim \text{Binomial}(N_i, t_i)$. Here t_i is the deterministic compression factor of prior mass X_{i-1} to X_i , which coincides with the probability that a randomly selected point sampled from the constrained prior $\pi|_{\mathcal{X}_{i-1}}$ falls into the level set \mathcal{X}_i . This allows for constructing a Monte Carlo estimator of the compression factor

$$\hat{t}_i = \frac{\hat{n}_i^{\mathcal{X}}}{N_i}, \quad (28)$$

leading to a sequence of estimators for the constrained prior masses

$$\hat{X}_i = \hat{X}_{i-1} \hat{t}_i \quad \text{with} \quad \hat{X}_0 = 1. \quad (29)$$

The corresponding estimator for the prior mass contained in slice i is estimated as $\hat{S}_i = \hat{X}_{i-1} - \hat{X}_i$. Unrolling the recursion, this yields

$$\hat{X}_i = \prod_{k=1}^i \hat{t}_k, \quad \text{and} \quad \hat{S}_i = (1 - \hat{t}_i) \prod_{k=1}^{i-1} \hat{t}_k, \quad (30)$$

with $\hat{t}_M = t_M = 0$ and $\hat{X}_M = X_M = 0$ by convention.

For $i < M$, the binomial distribution of $\hat{n}_i^{\mathcal{X}}$ implies that the estimator of the compression factor is unbiased $\mathbb{E}[\hat{t}_i] = t_i$ and its variance is

$$\text{Var}[\hat{t}_i] = \frac{\text{Var}[\hat{n}_i^{\mathcal{X}}]}{N_i^2} = \frac{t_i(1-t_i)}{N_i}. \quad (31)$$

Thus, the relative uncertainty

$$\varepsilon_{t_i} := \frac{\sqrt{\text{Var}[\hat{t}_i]}}{t_i} = \sqrt{\frac{1-t_i}{t_i N_i}} \quad (32)$$

of the compression factors is proportional to $1/\sqrt{N_i}$. This, in turn, determines the relative uncertainty of the estimator of the constrained prior mass.

$$\varepsilon_{\hat{X}_i}^2 = \sum_{k=1}^i \varepsilon_{t_k}^2 + \mathcal{O}(\varepsilon_t^4). \quad (33)$$

A more detailed uncertainty analysis is provided in Section [III B 2](#).

Crucially, all points that fall within the slice \mathcal{S}_i , follow the prior distribution constrained to \mathcal{S}_i , i.e.

$$\Theta | \Theta \in \mathcal{S}_i \sim \pi|_{\mathcal{S}_i} \quad \text{for} \quad \Theta \sim \pi|_{\mathcal{X}_{i-1}}. \quad (34)$$

This allows to extract valid prior samples $\{\Theta_{i,\ell}^{\mathcal{S}}\}_{\ell=1}^{\hat{n}_i^{\mathcal{S}}}$ from each slice. Analogously to $\hat{n}_i^{\mathcal{X}}$ in Equation (27), $\hat{n}_i^{\mathcal{S}}$ denotes the number of points falling into slice i , with

$$\hat{n}_i^{\mathcal{S}} = \begin{cases} N_i - \hat{n}_i^{\mathcal{X}} = N_i(1 - \hat{t}_i), & i < M, \\ \hat{n}_{M-1}^{\mathcal{X}} = N_{M-1}\hat{t}_{M-1}, & i = M. \end{cases} \quad (35)$$

Note that we will assume the thresholds and the number N_i of points generated in \mathcal{X}_{i-1} are chosen such that enough points fall into each slice, i.e. $\hat{n}_i^{\mathcal{S}} \gg 1$.

The complete procedure is summarized in Algorithm 1, which returns the constructed slices, the corresponding prior mass estimates, and a valid prior sample in each slice.

Algorithm 1 Slicing

Input: number of slices M

1: Set $\hat{X}_0 = X_0 = 1$, $\phi_0 = 0$ and $\mathcal{X}_0 = \Omega$

2: **for** $i = 1, \dots, M-1$ **do**

3: choose threshold $\phi_i > \phi_{i-1}$ as described in the text

4: set \mathcal{X}_i and $\mathcal{S}_i = \mathcal{X}_{i-1} \setminus \mathcal{X}_i$

5: Sample N_i points $\Theta_{i-1,k}^{\mathcal{X}} \sim \pi|_{\mathcal{X}_{i-1}}$

6: determine sample $\mathcal{S}_i \supset \{\Theta_{i,\ell}^{\mathcal{S}}\} \subset \{\Theta_{i-1,k}^{\mathcal{X}}\}$

7: compute compression \hat{t}_i and $\hat{X}_i = \hat{t}_i \hat{X}_{i-1}$ and $\hat{S}_i = \hat{X}_{i-1} - \hat{X}_i$

8: **end for**

9: set $\mathcal{S}_M = \mathcal{X}_{M-1}$, $\hat{S}_M = \hat{X}_{M-1}$

10: $\{\Theta_{M-1,\ell}^{\mathcal{X}}\} = \{\Theta_{M,\ell}^{\mathcal{S}}\} = \{\Theta_{M-2,k}^{\mathcal{X}}\} \setminus \{\Theta_{M-1,\ell}^{\mathcal{S}}\}$

Output: $\{\mathcal{X}_i, \hat{X}_i, \{\Theta_{i,k}^{\mathcal{X}}\}_{i=0}^{M-1}, \{\mathcal{S}_i, \hat{S}_i, \{\Theta_{i,\ell}^{\mathcal{S}}\}_{i=1}^M\}$

This construction adopts a frequentist view of volume estimation. A Bayesian alternative would model the compression factors t_i as Beta-distributed variables, based on the binomial sample. This would yield a hybrid strategy using Bayesian volume estimates while keeping Monte Carlo integration within each slice. In principle, a full Bayesian version is also possible if we can make prior assumptions on the target function within each slice.

B. Slice Monte Carlo Integration

The slicing algorithm outlined above provides a partition $\mathcal{S} = (\mathcal{S}_1, \dots, \mathcal{S}_M)$ of the parameter space, along with prior mass estimates and prior samples, of size $\hat{n}_i^{\mathcal{S}}$ for all slices $i = 1, \dots, M$. Although the function ϕ is used to generate the partition, the resulting partition can be used to perform stratified Monte Carlo integration on a different π -integrable function $L : \Omega \rightarrow \mathbb{R}$. Using the partition, we can rewrite the integral

$$\mathcal{Z} = \int L(\theta) d\pi(\theta) = \sum_{i=1}^M S_i \int L(\theta) d\pi|_{\mathcal{S}_i}(\theta) = \sum_{i=1}^M S_i \mathbb{E}_{\pi}[L(\Theta)|\Theta \in \mathcal{S}_i], \quad (36)$$

with the conditional mean defined as

$$\mathcal{Z}_{\mathcal{S}_i} = \mathbb{E}_{\pi}[L(\Theta)|\Theta \in \mathcal{S}_i] = \int L(\theta) d\pi|_{\mathcal{S}_i}(\theta) \quad (37)$$

We can use the samples within each slice generated by the slicing algorithm to estimate the integral over each slice *via* Monte Carlo integration. This motivates the following estimator, using slice volume estimates \hat{S}_i and prior samples $\{\Theta_{i,k}^{\mathcal{S}}\}$

$$\hat{\mathcal{Z}} := \sum_{i=1}^M \hat{S}_i \hat{\mathcal{Z}}_{\mathcal{S}_i} \quad \text{with} \quad \hat{\mathcal{Z}}_{\mathcal{S}_i} := \frac{1}{n_i} \sum_{k=1}^{n_i} L(\Theta_{i,k}^{\mathcal{S}}), \quad (38)$$

where we only selected a subset of points available in each slice. If a fixed fraction $\alpha_i \in (0, 1]$ of the available points is evaluated in each slice, then

$$n_i = \begin{cases} \alpha_i N_i (1 - \hat{t}_i) = \alpha_i \hat{n}_i^{\mathcal{S}}, & i < M, \\ \alpha_M N_{M-1} \hat{t}_{M-1} = \alpha_M \hat{n}_M^{\mathcal{S}}, & i = M. \end{cases} \quad (39)$$

In any case, we assume that at least one point falls within each slice, and that at least one point is evaluated, that is $1 \leq n_i \leq \hat{n}_i^{\mathcal{S}}$.

Especially if we assume that the slicing is performed with a cheap surrogate $\phi(\theta)$ of the target function $L(\theta)$, the advantage of this procedure is threefold:

a) The slicing and the determination of the corresponding constrained prior masses are based on the surrogate, for which it is easy to produce large sample sizes N_i , which are necessary for small uncertainties in the prior mass estimates. b) To generate uncorrelated samples from the constrained prior requires several (if not many) MC steps of some sort, where evaluations of the slicing function are necessary. This expensive step is performed on the surrogate function instead of the target function, allowing for better decorrelation of the generated samples. c) Once the slices and the corresponding prior masses are available with sufficient accuracy, we can estimate

the integral over the slices with much fewer sample points, i.e. the accuracy of the slice volume and the evaluated points of the target function are decoupled. The necessary number of point evaluations per slice depends on the variance of $L(\theta)$ within the slice, weighted by the slice's prior mass S_i . This can pose a significant advantage over standard reweighting methods, where volume uncertainty and the number of target evaluations are still coupled, as discussed in Section II C.

1. Unbiasedness

The estimator $\widehat{\mathcal{Z}}$ is unbiased, i.e. $\mathbb{E}[\widehat{\mathcal{Z}}] = \mathcal{Z}$. This follows from two observations: First, the estimator \hat{t}_i of the compression factor t_i is unbiased. Then

$$\widehat{S}_i = (1 - \hat{t}_i) \prod_{k=1}^{i-1} \hat{t}_k \quad (40)$$

is unbiased for all i , since $\hat{t}_1, \dots, \hat{t}_M$ are independent.

Second, the Monte Carlo estimator $\widehat{\mathcal{Z}}_{\mathcal{S}_i}$ is conditionally unbiased for the slice expectation $\mathbb{E}_\pi[L(\Theta)|\Theta \in \mathcal{S}_i]$.

This holds when conditioned on the sigma-field generated by the slice-membership indicators of all sampled points,

$$\mathcal{F}_{\mathcal{S}} := \sigma\left(\mathbb{1}_{\mathcal{S}_i}(\Theta_{i-1,k}^{\mathcal{X}}) : i = 1, \dots, M-1, k = 1, \dots, N_i\right),$$

i.e., when knowing which points fall into which sets.

Since the number n_i of selected points within slice \mathcal{S}_i and the corresponding volume estimator \widehat{S}_i are $\mathcal{F}_{\mathcal{S}}$ -measurable, they are constant under this conditioning. So we have

$$\mathbb{E}[\widehat{\mathcal{Z}}_{\mathcal{S}_i} | \mathcal{F}_{\mathcal{S}}] = \frac{1}{n_i} \sum_{k=1}^{n_i} \mathbb{E}[L(\Theta_{i,k}^{\mathcal{S}}) | \mathcal{F}_{\mathcal{S}}] = \mathbb{E}_\pi[L(\Theta) | \Theta \in \mathcal{S}_i] \quad (41)$$

Together this yields

$$\begin{aligned} \mathbb{E}[\widehat{\mathcal{Z}}] &= \sum_{i=1}^M \mathbb{E}\left[\mathbb{E}\left[\widehat{S}_i \widehat{\mathcal{Z}}_{\mathcal{S}_i} | \mathcal{F}_{\mathcal{S}}\right]\right] = \sum_{i=1}^M \mathbb{E}\left[\widehat{S}_i \mathbb{E}\left[\widehat{\mathcal{Z}}_{\mathcal{S}_i} | \mathcal{F}_{\mathcal{S}}\right]\right] \\ &= \sum_{i=1}^M \mathbb{E}[\widehat{S}_i] \mathbb{E}_\pi[L(\Theta) | \Theta \in \mathcal{S}_i] = \mathbb{E}_\pi[L(\Theta)] = \mathcal{Z} \end{aligned} \quad (42)$$

2. Variance

In addition to unbiasedness, we are interested in the variance of the estimator $\widehat{\mathcal{Z}}$. A detailed derivation is provided in Appendix A; here we present the general

structure and discuss its implications. The variance of $\widehat{\mathcal{Z}}$ can be expressed as

$$\text{Var}[\widehat{\mathcal{Z}}] = \sum_{i=1}^M \left(\Delta \mathcal{Z}_{\mathcal{S}_i}^2 \mathbb{E} \left[\frac{\widehat{S}_i^2}{n_i} \right] + \mathcal{Z}_{\mathcal{S}_i}^2 \text{Var}[\widehat{S}_i] + 2\text{Cov}[\widehat{S}_i, \widehat{X}_i] \mathcal{Z}_{\mathcal{S}_i} \mathcal{Z}_{\mathcal{X}_i} \right) \quad (43)$$

where $n_i \leq \widehat{n}_i^{\mathcal{S}}$ denotes the number of points selected in each slice for evaluation, with $\widehat{n}_i^{\mathcal{S}}$ defined in Equation (35), and

$$\mathcal{Z}_{\mathcal{A}} = \mathbb{E}_{\pi}[L(\Theta)|\Theta \in \mathcal{A}] \quad \text{and} \quad \Delta \mathcal{Z}_{\mathcal{A}}^2 = \text{Var}_{\pi}[L(\Theta)|\Theta \in \mathcal{A}], \quad (44)$$

denote the conditional expectation and variance over a non-empty region $\mathcal{A} \in \{\mathcal{X}_i\}_{i=0}^{M-1} \cup \{\mathcal{S}_i\}_{i=1}^M$. For $i = M$, the covariance contribution is interpreted as zero because $\widehat{X}_M = 0$ by convention; no conditional mean over \mathcal{X}_M is required.

This variance decomposition closely mirrors the structure of the nested sampling variance in Equation (20) that we provided in Section II B, but with key distinctions. In $S\ell MC$, discrete likelihood values are replaced by conditional expectations of the integrand within slices, and an additional term appears that accounts for intra-slice variability. While all terms depend on generally unknown properties of the integrand, they can be estimated from the available samples.

A central advantage of $S\ell MC$ compared to standard reweighting techniques is the decoupling of volume estimation from function evaluation. The variance contribution from volume uncertainty, captured in the second and third terms, can be made arbitrarily small by increasing the number of samples N_i , without incurring additional evaluations of the target function L . In contrast, the first term, arising from the variance of L within each slice, can be reduced by evaluating more points per slice. If n_i is constant, it can just be pulled out of the expectation. On the other hand, if we choose to evaluate a deterministic fraction $\alpha_i \in (0, 1]$ of the points available per slice, using Equation (39) gives

$$\mathbb{E} \left[\frac{\widehat{S}_i^2}{n_i} \right] = \begin{cases} \frac{1}{\alpha_i N_i} \frac{S_i}{X_{i-1}} \mathbb{E}[\widehat{X}_{i-1}^2], & i < M, \\ \frac{1}{\alpha_M N_{M-1}} \frac{S_M}{X_{M-2}} \mathbb{E}[\widehat{X}_{M-2}^2], & i = M. \end{cases} \quad (45)$$

This flexibility enables efficient resource allocation: volume estimation can be refined independently of the function evaluation budget. $S\ell MC$ is therefore especially well suited for problems where the integrand exhibits low variance within each slice, as high-accuracy integration can be achieved with minimal function evaluations. To achieve this, the slicing function ϕ should ideally act as a surrogate for the integrand L , such that L exhibits low variability within each slice.

3. Redrawing Points for Given Thresholds

In practice, it is often beneficial to be able to redraw points for given thresholds, to increase the accuracy of the volume estimates, or to generate more points within each slice. Different slicing runs, which have the same thresholds, can be easily combined. Each slicing run r with thresholds $\{\phi_j\}$, has samples $\{\Theta_{j,k}^{\mathcal{X},(r)}\}$ within the level sets $\{\mathcal{X}_j^{(r)}\}$. Assuming that the samples are independent for each run, we can simply pool them at each step of the algorithm

$$\{\Theta_{i,k}^{\mathcal{X}}\} = \bigcup_r \{\Theta_{i,k}^{\mathcal{X},(r)}\} \quad \text{and} \quad \{\Theta_{i,k}^{\mathcal{S}}\} = \bigcup_r \{\Theta_{i,k}^{\mathcal{S},(r)}\}, \quad (46)$$

and thereby increase the effective sample size to $N_i = \sum_r N_i^{(r)}$, and enhance the estimate of the updated compression factors

$$\hat{t}_i = \frac{\hat{n}_i^{\mathcal{X}}}{N_i} \quad \text{with} \quad \hat{n}_i^{\mathcal{X}} = \sum_r \hat{n}_i^{\mathcal{X},(r)}. \quad (47)$$

The rest of the analysis remains the same. An adaptation of this procedure for the case of different thresholds is provided in Appendix B.

4. Posterior Expectations and Posterior Samples

If the target function L is non-negative, we may interpret it as a likelihood function. Then the integral \mathcal{Z} is the evidence. In this case, it is also possible to compute the expectation value of a function $g : \Omega \rightarrow \mathbb{R}$ with respect to the posterior distribution $dp(\theta) = L(\theta) d\pi(\theta) / \mathcal{Z}$

$$\mathcal{G} = \int_{\Omega} g(\theta) \frac{L(\theta)}{\mathcal{Z}} d\pi(\theta) = \sum_{i=1}^M S_i \int g(\theta) \frac{L(\theta)}{\mathcal{Z}} d\pi|_{\mathcal{S}_i}(\theta) \quad (48)$$

using SLMC with the previously determined sample $\{\Theta_{i,k}^{\mathcal{S}}\}$ of the constraint prior

$$\hat{\mathcal{G}} = \sum_{i=1}^M \frac{\hat{S}_i}{n_i} \sum_{k=1}^{n_i} g(\Theta_{i,k}^{\mathcal{S}}) \frac{L(\Theta_{i,k}^{\mathcal{S}})}{\hat{\mathcal{Z}}} \quad (49)$$

Similar to NS, the slicing procedure naturally induces weighted posterior representatives

$$p_{i,k} := \frac{\hat{S}_i L(\Theta_{i,k}^{\mathcal{S}})}{n_i \hat{\mathcal{Z}}}, \quad (50)$$

which can be used to express the posterior expectation differently

$$\hat{\mathcal{G}} = \sum_{i=1}^M \sum_{k=1}^{n_i} g(\Theta_{i,k}^{\mathcal{S}}) p_{i,k}. \quad (51)$$

Here $p_{i,k}$ is the probability for a parameter value θ in a small volume of size ΔV_i centered at $\Theta_{i,k}^{\mathcal{S}}$, with $\Delta V_i \approx S_i/n_i$. Note that the number of points n_i evaluated for g and L in slice i can be adjusted depending on the variability of $g(\theta) \cdot p(\theta)$.

Beyond weighted representatives, $S\ell$ MC also enables the generation of equally weighted samples from the posterior via approximate rejection sampling. For that purpose, we define the piecewise-constant envelope

$$L^{\mathcal{S}} := \sum_{i=1}^M L_{\mathcal{S}_i}^{\max} \cdot \mathbb{1}_{\mathcal{S}_i}, \quad L_{\mathcal{S}_i}^{\max} := \max_{\theta \in \mathcal{S}_i} L(\theta). \quad (52)$$

As $L_{\mathcal{S}_i}^{\max}$ is typically unknown, we have to estimate it as $\hat{L}_{\mathcal{S}_i}^{\max} := \max\{L(\Theta_{i,k}^{\mathcal{S}})\}$ to obtain an estimated envelope $\hat{L}^{\mathcal{S}}$.

To sample from the posterior, we first draw from the approximate (unnormalized) distribution $\hat{L}^{\mathcal{S}}$ with prior distribution π using the estimated volumes \hat{S}_i (see Appendix C), and then apply rejection sampling within the selected slice \mathcal{S}_i . The acceptance probability is proportional to $L(\theta)/L_{\mathcal{S}_i}^{\max}$, from which it can be seen that the efficiency of this step depends on the within-slice variability of L .

$S\ell$ MC thus combines the variance-reduction benefits of stratification with the computational efficiency of surrogate-assisted reweighting, and provides a principled framework for adaptive slice selection and evaluation budgeting, while additionally enabling the generation of posterior samples.

IV. NUMERICAL ANALYSIS

To assess the performance of $S\ell$ MC, we compare it to Nested Sampling (NS), reweighting with NS (RW), and Monte Carlo importance sampling (IS) on controlled benchmark problems where the surrogate quality can be varied systematically. For NS and RW, we use Skilling’s deterministic prior-mass assignment $X_i = \exp(-i/N_{\text{live}})$ to obtain point estimators \hat{Z} . Details on the numerical setup for the respective methods are provided in Appendix D. The goal is to compare how the different estimators translate surrogate mismatch into the required number of target evaluations and assess the robustness of the respective methods to surrogate-target mismatch.

A. Benchmark models

The benchmark models are Gaussian surrogate-target pairs. Throughout the benchmark, $\Omega = B_1(0) \subset \mathbb{R}^d$ is the unit ball and π is the flat prior on Ω . The Gaussian parameters are chosen such that both ϕ and L are well contained in Ω , so boundary effects are negligible and the evidence $\mathcal{Z} = \mathbb{E}_\pi[L]$ defined in Equation (1) is given by the corresponding full-space Gaussian integral, which can be computed in closed form. Let

$$\varphi_d(\theta; \mu, \Sigma) := \exp \left[-\frac{1}{2} (\theta - \mu)^\top \Sigma^{-1} (\theta - \mu) \right] \quad (53)$$

denote an unnormalized Gaussian density on \mathbb{R}^d . For simplicity we choose an isotropic Gaussian as surrogate

$$\phi(\theta) = \varphi_d(\theta; \mu_\phi, \sigma_\phi^2 I_d), \quad (54)$$

chosen with mean $\mu_\phi = 0$ and variance $\sigma_\phi^2 = 2.5 \times 10^{-5}$ (standard deviation $\sigma_\phi = 0.005$).

We consider two target families – shift and anisotropy. The shift benchmark varies the relative mean displacement while keeping the variances isotropic with $\sigma_L^2 = \sigma_\phi^2$,

$$L_{\text{shift}}(\theta; b) = \varphi_d(\theta; \mu_L, \sigma_L^2 I_d), \quad b = \frac{\|\mu_L - \mu_\phi\|}{\sigma_L}. \quad (55)$$

The anisotropy benchmark fixes the means $\mu_L = \mu_\phi$ and varies

$$\begin{aligned} L_{\text{aniso}}(\theta; a) &= \varphi_d(\theta; \mu_L, \Sigma_L(a)), \\ \Sigma_L(a) &= \sigma_\phi^2 \text{diag}(\underbrace{a^2, \dots, a^2}_{\lfloor d/2 \rfloor}, \underbrace{a^{-2}, \dots, a^{-2}}_{\lceil d/2 \rceil}), \quad a \geq 1. \end{aligned} \quad (56)$$

Thus, one half of the coordinate directions is stretched and the other half is compressed. Note that an isotropic mismatch would only influence the performance of IS, while the other methods are invariant to isotropic scaling of the target.

Thus the shift family probes mean mismatch, while the anisotropy family probes covariance mismatch. For the even dimensions used below, the product of all target widths in the anisotropy benchmark is independent of a . For each mismatch setting, the exact value \mathcal{Z} is used to report relative errors $\delta := |\hat{\mathcal{Z}} - \mathcal{Z}| / \mathcal{Z}$.

B. Benchmarking procedure

We compare the above methods by evaluating their relative error as a function of the target-function evaluation cost

$$Q := \#\{\text{required evaluations of } L\}. \quad (57)$$

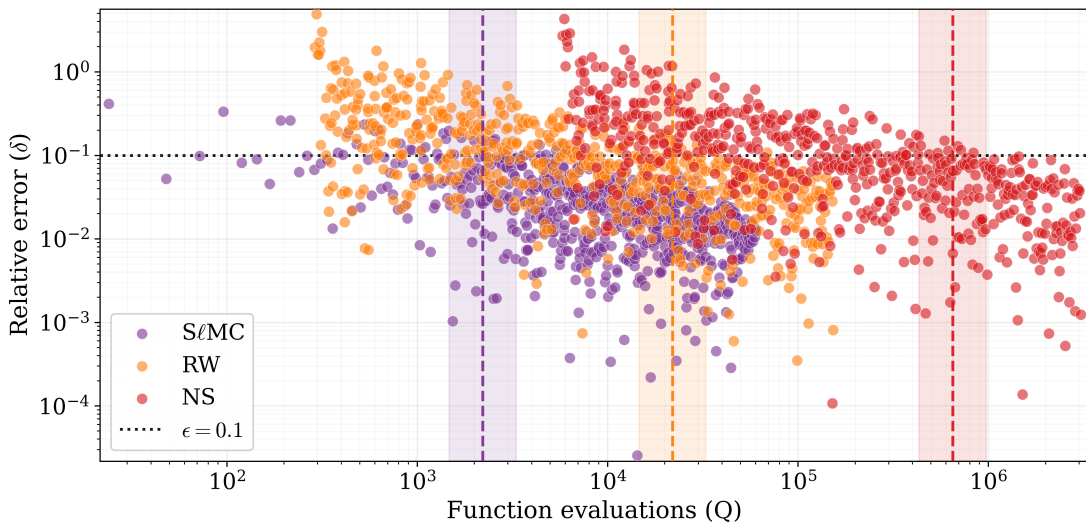


FIG. 1: Relative error δ as a function of target-evaluation cost Q for the anisotropy benchmark at $a = 2.4$ in $d = 2$, with detected convergence windows for $S\ell MC$ (purple), RW (orange), and NS (red). Transparent bands indicate the first local cost window in which the empirical success probability exceeds the criterion $\delta \leq \epsilon$ with $\epsilon = 0.1$, $p = 0.9$, and window factor $w = 1.5$ (see Appendix D). Dashed vertical lines mark the corresponding estimates of Q^* for $S\ell MC$, RW, and NS.

Evaluations of ϕ are treated as negligible and are not counted in Q . For a fixed cost Q , the relative error $\delta(Q)$ is random because each method is stochastic. Writing $\mathbb{P}[\cdot]$ for the probability distribution at fixed Q for the different methods, we define the minimal required cost for a tolerance ϵ and success probability p as

$$Q^*(\epsilon, p) = \min \{Q : \mathbb{P}[\delta(Q) \leq \epsilon] \geq p\} , \quad (58)$$

which is the minimal number of point evaluations of the target function required to achieve a relative error of at most ϵ with probability at least p . For $S\ell MC$, RW, and NS, repeated runs at different budgets produce empirical pairs (Q_j, δ_j) , which form an error–cost scatter plot as illustrated in Figure 1. We estimate Q^* from these empirical pairs by a window-based convergence criterion and quantify uncertainty by bootstrap resampling. The method-specific numerical setup, cost mappings, and estimation procedure are described in Appendix D. For IS, Q^* is obtained analytically using the central limit theorem; see Appendix E.

C. Results

We report benchmark results for $d = 2$, $d = 8$, and $d = 30$. For clarity, the $d = 2$ panels use $\epsilon = 0.1$, while the $d = 8$ and $d = 30$ panels use $\epsilon = 0.2$. All panels in

Figure 2 show the required cost $Q^*(\epsilon, p = 0.9)$, with bootstrap 16th/84th percentile bands for $S\ell MC$, RW, and NS (see Appendix D), and analytical CLT values for IS (see Appendix E). For IS we additionally show the effect of scaling the surrogate proposal variance by using

$$\phi_\eta(\theta) = \varphi_d(\theta; \mu_\phi, \eta\sigma_\phi^2 I_d), \quad \eta \in \{0.7, 1.0, 1.3\}. \quad (59)$$

The other methods are invariant to isotropic scaling of the surrogate, so only one curve is shown for each of $S\ell MC$, RW, and NS.

NS forms a constant baseline in these plots because it does not depend on the surrogate. Its cost is therefore independent of the surrogate-target mismatch by construction. The larger absolute level of NS compared with RW mainly reflects the cost model in Appendix D 1: RW evaluates L on the stored surrogate-NS representatives, whereas direct NS pays the constrained-replacement overhead c_{NS} during target-based sampling.

In the anisotropy benchmark, the top-row panels of Figure 2 show Q^* as a function of the anisotropy parameter a . Across all dimensions, IS has the lowest cost when a is close to one, as expected from its favorable behavior when the proposal is nearly identical to the target. This advantage is fragile: as soon as the surrogate is too narrow in one target direction, the importance-weight variance diverges. For the unscaled proposal, the finite-variance condition derived in Appendix E translates to $a < \sqrt{2}$ for the stretched directions; with proposal variance scale η , this boundary becomes $a < \sqrt{2\eta}$. Thus the IS curves terminate at predictable finite-variance boundaries, and the deterioration before those boundaries is particularly pronounced.

$S\ell MC$ and RW are more robust because they do not rely on a single global importance density with finite weight variance. Instead, both methods use the surrogate to partition the parameter space and distribute samples across the induced level sets, so their cost grows more gracefully as the surrogate-target mismatch increases. Both methods become more expensive as a increases, since the target varies more strongly inside the surrogate-induced slices, but $S\ell MC$ remains consistently below RW over the tested range. This is the practical effect of decoupling slice-volume estimation from target evaluation: $S\ell MC$ can spend many cheap surrogate samples on the partition and volume estimation, while only the selected integration points require expensive evaluations of L . As the mismatch and thus the within-slice variance increase $S\ell MC$ gets closer to RW, as many points within each slice are needed to obtain a small relative error. This behavior is consistent across all investigated dimensions. However, for increasing dimension the mismatch leads to higher absolute Q^* values and more sensitive behavior with respect to the mismatch.

In the shift benchmark, the bottom-row panels of Figure 2 show Q^* as a function of the shift parameter b . Here the surrogate and target have the same shape, but their centers are displaced. IS again starts with the lowest cost near perfect agreement; for

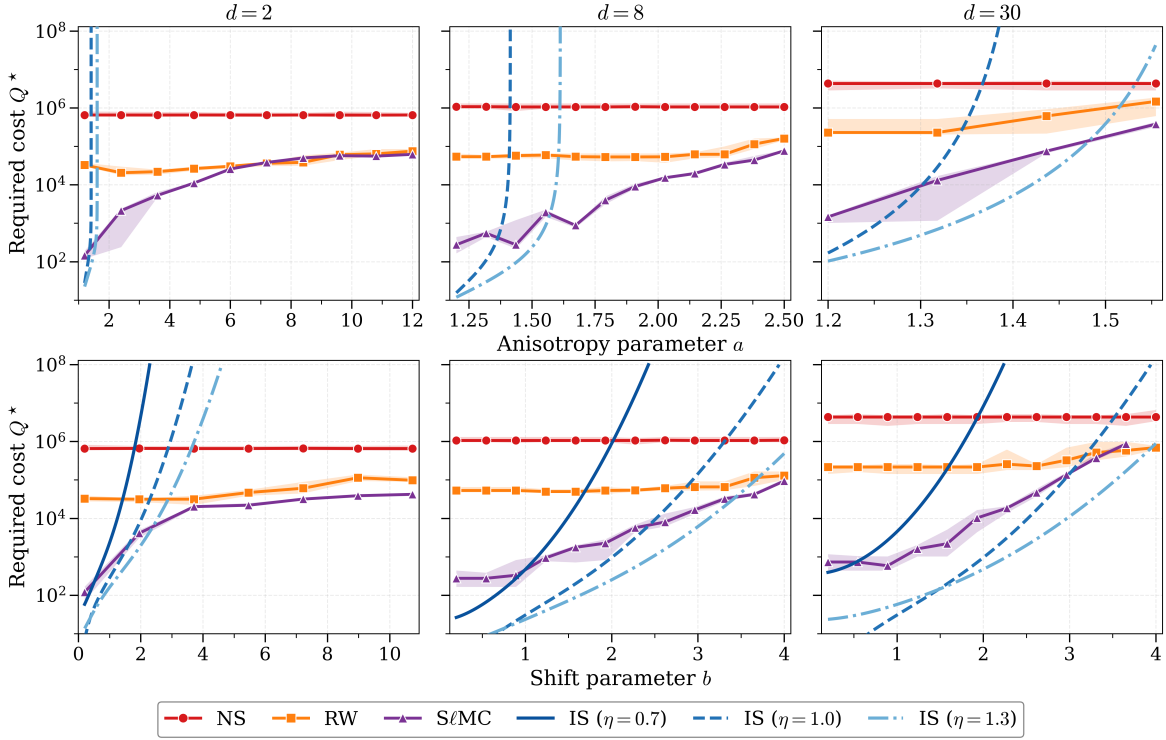


FIG. 2: Required target-evaluation cost Q^* across benchmark families and dimensions. The top row shows the anisotropy benchmark and the bottom row the shift benchmark, with columns corresponding to $d = 2$, $d = 8$, and $d = 30$. Shaded bands show bootstrap 16th/84th percentiles ($n_{\text{boot}} = 500$) for $S\ell\text{MC}$, RW, and NS. IS curves are analytical CLT estimates for proposal variances $\eta\sigma_\phi^2$ with $\eta \in \{0.7, 1.0, 1.3\}$; in the anisotropy benchmark the unscaled IS proposal has its variance-divergence boundary at $a = \sqrt{2}$. The $d = 2$ column uses $\epsilon = 0.1$, while the $d = 8$ and $d = 30$ columns use $\epsilon = 0.2$, as annotated in each panel.

the unscaled proposal its normalized variance grows like $\exp(b^2)$ in the isotropic shift case (Appendix E), and the variance-scaled proposals retain the same exponential sensitivity. This is less abrupt than the anisotropy benchmark because there is no finite-variance boundary; nevertheless, the cost eventually becomes enormous as the high-mass regions of surrogate and target separate.

$S\ell\text{MC}$ and RW are more stable under this mismatch because their surrogate-based partitions still place samples across the relevant level sets. Their costs increase with b , but the growth is much slower than for IS over the range shown, and again $S\ell\text{MC}$ remains below RW. This is consistent with the same decoupling principle: the surrogate partition can still be estimated cheaply, while target evaluations are allocated only to estimate the contributions within the resulting slices.

The two benchmark families highlight complementary failure modes. IS is optimal only when the surrogate is very accurate: it is extremely sensitive to shape mismatch, where a single overly narrow surrogate direction can make the variance infinite, and it deteriorates exponentially under pure position mismatch. RW and $S\ell$ MC are more robust because they use the surrogate to partition the parameter space rather than using a single global importance density.

$S\ell$ MC is typically more efficient than RW because the expensive target evaluations are decoupled from the surrogate-based volume estimation, but this advantage naturally shrinks when large mismatch forces many target evaluations within each slice. This also explains why the two curves approach each other at larger mismatch. When the target varies strongly within the surrogate-induced slices, $S\ell$ MC must evaluate many target points per slice, so within-slice target variance dominates and slice-volume uncertainty becomes less relevant. In the same regime, the volume uncertainty in RW becomes small and the remaining uncertainty stems from the target variance along the surrogate level sets. So $S\ell$ MC and RW have the same dominant source of uncertainty. Additionally, the effective point weights of RW and $S\ell$ MC become similar, when RW and $S\ell$ MC use a comparable number of points per volume. For small mismatch, in contrast, $S\ell$ MC can achieve low error with few target evaluations per slice due to the decoupling of volume uncertainty and target evaluations, while RW still pays for the coupled volume-estimation and target-evaluation mechanism.

NS, finally, remains the surrogate-independent reference method: its cost is flat across mismatch parameters and higher than RW in the present comparison because direct constrained sampling carries the additional target-evaluation overhead.

Together, the results show that $S\ell$ MC turns surrogate quality into reduced target-evaluation cost while retaining considerably more robustness to mismatch than direct importance sampling.

V. CONCLUSION AND OUTLOOK

We have introduced Slice Monte Carlo integration ($S\ell$ MC) as a surrogate-informed integration method that uses a Nested Sampling-like construction to partition the parameter space into slices adapted to the surrogate level sets. The partition and the slice volumes are estimated using the cheap surrogate, while the expensive target function is evaluated only for the Monte Carlo estimates within the slices.

The central advantage is the decoupling of slice-volume estimation from target evaluation. Standard reweighting with Nested Sampling uses the surrogate to avoid expensive constrained sampling, but target evaluations remain tied to the quadrature resolution. $S\ell$ MC separates these two tasks: many surrogate samples can refine the

slice volumes, while the number of target evaluations can be chosen independently according to the integration budget. This additional degree of freedom explains the improved performance over reweighting observed in the benchmark problems.

Compared with classical importance sampling, $S\ell$ MC is substantially more robust to surrogate-target mismatch. Importance sampling is most efficient when the surrogate proposal is already very close to the target, but it deteriorates rapidly when surrogate-target mismatch occurs. $S\ell$ MC instead uses the surrogate only to define a partition of the parameter space and estimates the target contribution within each slice directly, avoiding the severe failure modes of importance sampling. The price is that, in the ideal case of nearly perfect surrogate-target agreement, direct importance sampling can require fewer target evaluations. In realistic applications, however, surrogate information is rarely perfect, and robustness to mismatch is often more valuable than optimal performance in this limiting case.

The present numerical study used a deliberately simple and uniform protocol for the number of target evaluations per slice setting $n_i = n$ for all slices $i = 1, \dots, M$. A natural extension is an adaptive allocation strategy in which the number of evaluated points is chosen from estimates of the target variance within each slice, as in classical stratified Monte Carlo methods¹⁵. This could be combined with control-variate ideas from multifidelity and multilevel Monte Carlo methods²⁷⁻²⁹, for example by estimating slice-wise surrogate-target correlations. More speculatively, if several surrogate models of increasing fidelity are available, one could transfer or refine the slice partition across fidelity levels, to obtain a multilevel version of $S\ell$ MC.

$S\ell$ MC is particularly attractive because the hard constrained-sampling task is performed on the cheap surrogate, while the resulting slices are then used for a stratified integration of the expensive target. This makes the method relevant for applications where low-fidelity physical models are readily available^{7,8}, where simplified energy landscapes can guide expensive partition-function calculations^{10,12}, or where machine-learned surrogate models approximate costly high-fidelity evaluations^{20-22,24}. Overall, $S\ell$ MC provides a robust and flexible framework for surrogate-informed Bayesian evidence integration when the surrogate is useful but not perfectly reliable.

Appendix A: Variance of Slice Integration

The aim of this section is the computation of the variance of the $S\ell$ MC estimator of the evidence \mathcal{Z} . Recall that the estimator of the constrained prior mass is given by $\hat{X}_{i-1} = \prod_{k=1}^{i-1} \hat{t}_k$ with independent compression factors $N_k \hat{t}_k \sim \text{Binomial}(N_k, X_k / X_{k-1})$ for $k < M$, with $\hat{X}_0 = X_0 = 1$ and $\hat{X}_M = X_M = 0$ by convention. The estimator of the slice volume is $\hat{S}_k = \hat{X}_{k-1} - \hat{X}_k$. From that, we

obtain

$$\begin{aligned}\mathbb{E}[\widehat{X}_{i-1}] &= \prod_{k=1}^{i-1} \mathbb{E}[\widehat{t}_k] = \prod_{k=1}^{i-1} \frac{X_k}{X_{k-1}} = X_{i-1} \\ \mathbb{E}[\widehat{X}_{i-1}^2] &= X_{i-1}^2 + \text{Var}[\widehat{X}_{i-1}]\end{aligned}\tag{A1}$$

with variance

$$\begin{aligned}\text{Var}[\widehat{X}_{i-1}] &= \prod_{k=1}^{i-1} \left(\frac{1}{N_k} \frac{X_k}{X_{k-1}} \left(1 - \frac{X_k}{X_{k-1}} \right) + \frac{X_k^2}{X_{k-1}^2} \right) - \prod_{k=1}^{i-1} \frac{X_k^2}{X_{k-1}^2} \\ &= X_{i-1}^2 \sum_{k=1}^{i-1} \frac{S_k}{N_k X_k} + \mathcal{O}\left(\frac{1}{N^2}\right).\end{aligned}\tag{A2}$$

For $i < M$, we can compute the variance of the slice estimator \widehat{S}_i by using the independence of \widehat{X}_{i-1} and \widehat{t}_i

$$\begin{aligned}\text{Var}[\widehat{S}_i] &= \text{Var}[\widehat{X}_{i-1}(1-\widehat{t}_i)] \\ &= \text{Var}[\widehat{X}_{i-1}]\text{Var}[1-\widehat{t}_i] + \text{Var}[\widehat{X}_{i-1}]\mathbb{E}[1-\widehat{t}_i]^2 + \text{Var}[1-\widehat{t}_i]\mathbb{E}[\widehat{X}_{i-1}]^2 \\ &= \text{Var}[\widehat{X}_{i-1}] \left(\frac{1}{N_i} \frac{S_i}{X_{i-1}} \left(1 - \frac{S_i}{X_{i-1}} \right) + \frac{S_i^2}{X_{i-1}^2} \right) + \frac{S_i X_i}{N_i} \\ &= S_i^2 \sum_{k=1}^{i-1} \frac{S_k}{N_k X_k} + \frac{S_i X_i}{N_i} + \mathcal{O}\left(\frac{1}{N^2}\right).\end{aligned}\tag{A3}$$

For the final slice, $\widehat{S}_M = \widehat{X}_{M-1}$, so $\text{Var}[\widehat{S}_M] = \text{Var}[\widehat{X}_{M-1}]$. Another quantity we need for computing $\text{Var}[\widehat{Z}]$, is the covariance between the estimators \widehat{S}_i and \widehat{X}_i for $i < M$, which is

$$\begin{aligned}\text{Cov}[\widehat{S}_i, \widehat{X}_i] &= \text{Cov}[\widehat{X}_{i-1}(1-\widehat{t}_i), \widehat{X}_{i-1}\widehat{t}_i] \\ &= \mathbb{E}[\widehat{X}_{i-1}^2]\text{Cov}[1-\widehat{t}_i, \widehat{t}_i] + \text{Var}[\widehat{X}_{i-1}]\mathbb{E}[1-\widehat{t}_i]\mathbb{E}[\widehat{t}_i] \\ &= \text{Var}[\widehat{X}_{i-1}] \left(\mathbb{E}[\widehat{t}_i] - \mathbb{E}[\widehat{t}_i]^2 \right) - \text{Var}[\widehat{t}_i]\mathbb{E}[\widehat{X}_{i-1}^2] \\ &= \frac{X_i}{X_{i-1}} \left(1 - \frac{X_i}{X_{i-1}} \right) \left(\text{Var}[\widehat{X}_{i-1}] - \frac{1}{N_i} \mathbb{E}[\widehat{X}_{i-1}^2] \right) \\ &= X_i S_i \left(\sum_{k=1}^{i-1} \frac{S_k}{N_k X_k} - \frac{1}{N_i} \right) + \mathcal{O}\left(\frac{1}{N^2}\right).\end{aligned}\tag{A4}$$

The previous computations allow for determining the variance of the estimator $\widehat{Z} = \sum_{i=1}^M \widehat{S}_i \widehat{Z}_{\mathcal{J}_i}$, yielding

$$\text{Var}[\widehat{Z}] = \sum_{i=1}^M \text{Var}[\widehat{S}_i \widehat{Z}_{\mathcal{J}_i}] + 2 \sum_{\substack{i,j=1 \\ i < j}}^M \text{Cov}[\widehat{S}_i \widehat{Z}_{\mathcal{J}_i}, \widehat{S}_j \widehat{Z}_{\mathcal{J}_j}].\tag{A5}$$

We again can compute the individual terms by conditioning on the sigma-field $\mathcal{F}_{\mathcal{S}}$, which encodes the slice-membership information of the sampled points. By using the law of total variance and the $\mathcal{F}_{\mathcal{S}}$ -measurability of \widehat{S}_i and n_i , we get

$$\begin{aligned}\text{Var}[\widehat{S}_i \widehat{\mathcal{Z}}_{\mathcal{S}_i}] &= \mathbb{E}[\text{Var}[\widehat{S}_i \widehat{\mathcal{Z}}_{\mathcal{S}_i} | \mathcal{F}_{\mathcal{S}}]] + \text{Var}[\mathbb{E}[\widehat{S}_i \widehat{\mathcal{Z}}_{\mathcal{S}_i} | \mathcal{F}_{\mathcal{S}}]] \\ &= \text{Var}[L(\Theta) | \Theta \in \mathcal{S}_i] \mathbb{E}\left[\frac{\widehat{S}_i^2}{n_i}\right] + \mathbb{E}[L(\Theta) | \Theta \in \mathcal{S}_i]^2 \text{Var}[\widehat{S}_i]\end{aligned}\quad (\text{A6})$$

and for the covariance

$$\begin{aligned}\text{Cov}[\widehat{S}_i \widehat{\mathcal{Z}}_{\mathcal{S}_i}, \widehat{S}_j \widehat{\mathcal{Z}}_{\mathcal{S}_j}] &= \mathbb{E}[\text{Cov}[\widehat{S}_i \widehat{\mathcal{Z}}_{\mathcal{S}_i}, \widehat{S}_j \widehat{\mathcal{Z}}_{\mathcal{S}_j} | \mathcal{F}_{\mathcal{S}}]] \\ &\quad + \text{Cov}[\mathbb{E}[\widehat{S}_i \widehat{\mathcal{Z}}_{\mathcal{S}_i} | \mathcal{F}_{\mathcal{S}}], \mathbb{E}[\widehat{S}_j \widehat{\mathcal{Z}}_{\mathcal{S}_j} | \mathcal{F}_{\mathcal{S}}]].\end{aligned}\quad (\text{A7})$$

Using again the $\mathcal{F}_{\mathcal{S}}$ -measurability and the independence of the samples within each slice, we get for the first term for $i \neq j$

$$\mathbb{E}[\text{Cov}[\widehat{S}_i \widehat{\mathcal{Z}}_{\mathcal{S}_i}, \widehat{S}_j \widehat{\mathcal{Z}}_{\mathcal{S}_j} | \mathcal{F}_{\mathcal{S}}]] = \mathbb{E}[\widehat{S}_i \widehat{S}_j \text{Cov}[\widehat{\mathcal{Z}}_{\mathcal{S}_i}, \widehat{\mathcal{Z}}_{\mathcal{S}_j} | \mathcal{F}_{\mathcal{S}}]] = 0 \quad (\text{A8})$$

and thus we get

$$\text{Cov}[\widehat{S}_i \widehat{\mathcal{Z}}_{\mathcal{S}_i}, \widehat{S}_j \widehat{\mathcal{Z}}_{\mathcal{S}_j}] = \mathcal{Z}_{\mathcal{S}_i} \mathcal{Z}_{\mathcal{S}_j} \text{Cov}[\widehat{S}_i, \widehat{S}_j]. \quad (\text{A9})$$

For $i < j$ we can write

$$\widehat{S}_j = \widehat{X}_i \prod_{k=i+1}^{j-1} \hat{t}_k (1 - \hat{t}_j), \quad (\text{A10})$$

and again, by using the independence of the compression factors, we obtain

$$\text{Cov}[\widehat{S}_i, \widehat{S}_j] = \text{Cov}[\widehat{S}_i, \widehat{X}_i] \mathbb{E}[1 - \hat{t}_j] \prod_{k=i+1}^{j-1} \mathbb{E}[\hat{t}_k] = \text{Cov}[\widehat{S}_i, \widehat{X}_i] \frac{S_j}{X_i}. \quad (\text{A11})$$

Evaluating the sum over j in the covariance term yields

$$\sum_{j=i+1}^M \text{Cov}[\widehat{S}_i \widehat{\mathcal{Z}}_{\mathcal{S}_i}, \widehat{S}_j \widehat{\mathcal{Z}}_{\mathcal{S}_j}] = \frac{\mathcal{Z}_{\mathcal{S}_i} \text{Cov}[\widehat{S}_i, \widehat{X}_i]}{X_i} \sum_{j=i+1}^M \mathcal{Z}_{\mathcal{S}_j} S_j = \mathcal{Z}_{\mathcal{S}_i} \mathcal{Z}_{\mathcal{X}_i} \text{Cov}[\widehat{S}_i, \widehat{X}_i]. \quad (\text{A12})$$

Altogether, this gives the final expression for the variance of the estimator $\widehat{\mathcal{Z}}$

$$\text{Var}[\widehat{\mathcal{Z}}] = \sum_{i=1}^M \left(\Delta \mathcal{Z}_{\mathcal{S}_i}^2 \mathbb{E}\left[\frac{\widehat{S}_i^2}{n_i}\right] + \mathcal{Z}_{\mathcal{S}_i}^2 \text{Var}[\widehat{S}_i] + 2 \text{Cov}[\widehat{S}_i, \widehat{X}_i] \mathcal{Z}_{\mathcal{S}_i} \mathcal{Z}_{\mathcal{X}_i} \right) \quad (\text{A13})$$

where n_i denotes the number of points selected in each slice, and

$$\mathcal{Z}_{\mathcal{A}} = \mathbb{E}_{\pi}[L(\Theta) | \Theta \in \mathcal{A}] \quad \text{and} \quad \Delta \mathcal{Z}_{\mathcal{A}}^2 = \text{Var}_{\pi}[L(\Theta) | \Theta \in \mathcal{A}], \quad (\text{A14})$$

denote the conditional expectation and variance over a non-empty region $\mathcal{A} \in \{\mathcal{X}_i\}_{i=0}^{M-1} \cup \{\mathcal{S}_i\}_{i=1}^M$. For $i = M$, the covariance contribution is interpreted as zero because $\widehat{X}_M = 0$ by convention; no conditional mean over \mathcal{X}_M is required.

Appendix B: Combining Runs and Redrawing

In practice, it can also be beneficial to combine results from multiple independent slicing runs to improve accuracy and robustness. Each slicing run r defines a valid partition of the parameter space via a sequence of slicing thresholds $\{\phi_j^{(r)}\}$, associated level sets $\{\mathcal{X}_j^{(r)}\}$, and corresponding samples $\{\Theta_{j,k}^{\mathcal{X},(r)}\}$. Multiple such runs can be combined to refine the partition and improve volume estimates by aggregating information across runs.

The combination procedure begins by forming a global list of thresholds $\{\phi_i\}$ from the union of all $\{\phi_j^{(r)}\}$, sorted in ascending order without duplication. For each ϕ_i , we collect all available samples from level sets corresponding to that threshold

$$\{\Theta_{i,k}^{\mathcal{X}}\} = \bigcup_{(r,j):\phi_j^{(r)}=\phi_i} \{\Theta_{j,k}^{\mathcal{X},(r)}\}. \quad (\text{B1})$$

This pooled sample is then used in a somewhat modified slicing algorithm (cf. Algorithm 1)

- Step 3 is modified to use the available sample $\{\Theta_{i-1,k}^{\mathcal{X}}\}$ from the previous level set \mathcal{X}_{i-1} .
- Step 4 selects a new threshold ϕ_i from the combined list, based on predefined criteria (e.g., the new threshold must not be too close to the previous one, such that sufficiently many points can fall within the thresholds).

If no points fall between two successive thresholds, the algorithm may skip over them. However, thresholds originating from a valid slicing run will eventually satisfy the selected slicing condition. The rest of the procedure follows the standard slicing logic, yielding updated slices, volume estimates, and filtered samples.

This approach enables reuse of already sampled points without introducing a bias. It can be used to refine the resolution of the slice partition by integrating new thresholds across runs, or redraw samples within a fixed partition to increase the number of points per slice, reducing the variance of volume estimates, and providing more samples for the intra-slice Monte Carlo estimation. In the special case where all runs share identical thresholds $\{\phi_j^{(r)}\} \equiv \{\phi_j\}$, the combination acts purely as a redrawing procedure. The samples in each slice are pooled, increasing the effective sample size $N_i = \sum_r N_i^{(r)}$, allowing higher accuracy in estimating slice volumes and expectations, as discussed in Section III B 3.

Appendix C: Drawing Random Points from the Posterior

The goal is to draw samples from the “expensive” target posterior PDF $p(\theta) = L(\theta)\pi(\theta)/\mathcal{Z}$ based on the rejection technique and the already stored sample $\{\Theta_{i,k}\}_{k=1}^{n_i}$ of parameter values in slice i , which are distributed according to the constrained prior PDF $\pi|_{\mathcal{S}_i}$. To this end, we need a simple envelope PDF $p^{(s)}(\Theta)$ that fulfills the condition

$$p(\theta) \leq \frac{\kappa}{\mathcal{Z}} p^{(s)}(\theta), \quad (\text{C1})$$

with some suitable parameter κ from which we can easily draw samples Θ^t . This proposed parameter point is then accepted with probability

$$P_{\text{acc}} = \frac{L(\Theta^t)\pi(\Theta^t)}{\kappa p^{(s)}(\Theta^t)}. \quad (\text{C2})$$

For the envelope, we choose the piecewise-constant function

$$p^{(s)}(\theta) = \sum_i a_i \widehat{S}_i \pi|_{\mathcal{S}_i}(\theta) \approx \sum_i a_i \pi(\theta) \mathbb{1}_{\mathcal{S}_i}[\theta] \quad \text{with} \quad \int p^{(s)}(\theta) dV_\theta = \sum_i a_i \widehat{S}_i \stackrel{!}{=} 1$$

The prior volume in slice \mathcal{S}_i is estimated by \widehat{S}_i . For slice i the condition reads

$$L(\Theta) \leq \kappa a_i,$$

according to Equation (C1). We can ignore the normalization condition for the coefficients a_i as it can be absorbed in κ . The coefficients a_i can be determined by using a small subset $I_i \subset \{\Theta_{i,k}\}_{k=1}^{n_i}$ of the predetermined parameter points in slice i and we use

$$\kappa a_i \approx L_i^{\max} := \max_{\Theta \in I_i} L(\Theta).$$

The acceptance probability for a proposed parameter value, given it lies in slice i , then simplifies to

$$P_i^{\text{acc}} = \frac{L(\Theta)}{L_i^{\max}}.$$

The probability that a parameter point Θ drawn from the envelope distribution falls into slice i is

$$P_i = \int_{\mathcal{S}_i} p^{(s)}(\theta) dV_\theta = \frac{L_i^{\max} \widehat{S}_i}{\sum_j L_j^{\max} \widehat{S}_j}. \quad (\text{C3})$$

The number of points $N_{\text{post},i}$ in slice i is multinomial with mean

$$\langle N_{\text{post},i} \rangle = N_{\text{post}} P_i, \quad (\text{C4})$$

where N_{post} is the total number of posterior points. Therefore, the random numbers

$$R_i := \frac{N_{\text{post},i}}{P_i} \quad (\text{C5})$$

have mean N_{post} and variance $\text{Var}[R_i] = N_{\text{post}}(1 - P_i)/P_i$. The actual numbers R_i can be used as a diagnostic tool for the performance of the run.

Now, drawing a parameter value Θ proceeds in two steps: first, we select a slice i with probability P_i and, within that slice, we draw a trial parameter point Θ^t according to the constrained prior. This parameter is accepted with probability P_i^{acc} . Drawing a random parameter value from the constrained prior can be strongly simplified, as we already have a large sample of stored parameter points with the correct distribution. So we merely have to select uniformly from the stored subset of points belonging to slice i , not just those that have been used to determine a_i . Therefore, it may happen that the condition in Equation (C1) is violated. This is the case if

$$L(\Theta) > L_i^{\text{max}}.$$

A remedy would be to set $L_i^{\text{max}} = L(\Theta)$, but that implies that the number of points collected so far in slice i is too small as compared to the number of points in the other slices (see Equations (C3) and (C4)). The ratio of the number of points in the other slices is still correct. The deficiency in slice i could be cured by the **greedy sampling**, i.e., by drawing selectively more points in slice i until $N_{\text{post},i}$ equals the mean value or until R_i is equal to the minimum R_j of the other slices.

But besides the number of points in the slices, also the distribution of points within slice i is no longer correct, due to the change of a_i . Therefore, the rejection step has to be repeated in that slice with the updated envelope. Note, however, that this step does not require additional target function evaluations.

Appendix D: Numerical Implementation Details

This appendix specifies how the empirical error–cost pairs used in Section IV are generated and how the method-specific cost mappings are defined. The common cost variable is the number of pointwise target evaluations Q , but each method has its own native control parameter, and therefore a different mapping from that parameter to Q .

1. Method setup and cost mappings

For IS, no empirical schedule is required because Q_{IS}^* is obtained analytically from the central limit theorem in Appendix E. The corresponding native control parameter is the number of importance samples N_{IS} ; each sample requires one evaluation of L , so $Q = N_{\text{IS}}$.

For $S\ell\text{MC}$ we construct the slices from the surrogate ϕ as in Section III A, with the same rule in every benchmark: using an independent pilot run, the thresholds ϕ_i are taken as the median surrogate value of the constrained-prior samples above ϕ_{i-1} , so every compression factor is $t_i \approx \frac{1}{2}$ (no slice holds more than half of the samples in \mathcal{X}_{i-1}). Each step uses $N_i = N_\phi$ surrogate draws, with $N_\phi = 5000$ for $d = 2$ and 4×10^4 for $d = 8, 30$. The number of slices M is an output of this construction, not a free parameter: starting from the lowest threshold, new slices are added until the running estimate of the surrogate integral stabilizes. Writing $\widehat{\mathcal{Z}}_\phi^{(i)}$ for the estimate after i slices, generation stops at the first slice for which

$$|\log \widehat{\mathcal{Z}}_\phi^{(i)} - \log \widehat{\mathcal{Z}}_\phi^{(i-1)}| < 10^{-3}, \quad (\text{D1})$$

i.e. a relative change of the estimate below $\sim 10^{-3}$; a final slice then collects the remaining mass. The resulting M grows with dimension ($M = 24, 55, 146$ for $d = 2, 8, 30$). All thresholds are fixed before any evaluations of L . The target is then evaluated at n_i points in slice i ; in the reported runs, the native control parameter is the equal allocation $n_i = n$, which is increased geometrically, so $Q = \sum_{i=1}^M n_i = Mn$.

For NS the native control parameter is the number of live points N_{live} , which we increase geometrically. Each run is terminated adaptively when the estimated fraction of evidence remaining in the live set falls below a tolerance

$$\frac{\langle L \rangle_{\text{live}} X_i}{\widehat{\mathcal{Z}}^{(i)}} < 10^{-3}, \quad X_i \approx \exp(-i/N_{\text{live}}), \quad (\text{D2})$$

where $\langle L \rangle_{\text{live}}$ is the mean likelihood of the current live points, X_i is Skilling's deterministic prior-mass estimate after i iterations, and $\widehat{\mathcal{Z}}^{(i)}$ is the running evidence estimate. To ensure termination, we also impose a maximum-iteration cap. We denote by K the resulting number of iterations, i.e. constrained replacements. For RW, this NS run is performed on the surrogate and L is evaluated on the K discarded surrogate-NS representatives and the final N_{live} live points, giving $Q = K + N_{\text{live}}$. For direct NS, the initial live points require N_{live} target evaluations and each constrained replacement has target-evaluation cost c_{NS} , giving $Q = N_{\text{live}} + c_{\text{NS}}K$. In the present Gaussian benchmarks, constrained points for NS can be sampled exactly from the relevant Gaussian level sets inside the prior ball. In general, however, c_{NS} depends on the problem, the dimension, and the constrained-sampling method and is thus

a complicated function of the complete problem setup.^{34,35,37} To respect this typical constraint, we set $c_{\text{NS}} = 20$, but note that this is only a heuristic choice to illustrate the overhead of target function evaluations in NS compared to RW.

Overall, the resulting target-evaluation costs are summarized as

$$Q = \begin{cases} N_{\text{IS}}, & \text{IS,} \\ \sum_{i=1}^M n_i, & \text{S}\ell\text{MC,} \\ K + N_{\text{live}}, & \text{RW,} \\ N_{\text{live}} + c_{\text{NS}}K, & \text{NS,} \end{cases} \quad (\text{D3})$$

2. Estimating the required computational budget

For S ℓ MC, RW, and NS, each run contributes a point (Q_j, δ_j) . The costs Q_j are obtained by sweeping each method's native control parameter—the per-slice sample count n for S ℓ MC and the number of live points N_{live} for NS and RW—over a geometric grid, starting from an initial value and multiplying by a fixed factor at each step up to a maximum, and mapping it to a cost through the relations in Equation (D3). To detect convergence robustly, we scan these candidate costs Q_j in increasing order and test a multiplicative local window of breadth $w > 1$,

$$Q \in \left[\frac{Q_j}{w}, wQ_j \right]. \quad (\text{D4})$$

We accept Q_j when the fraction of points in that window satisfying $\delta \leq \epsilon$ exceeds the success threshold p

$$\frac{\#\{k : \delta_k \leq \epsilon, Q_k \in [Q_j/w, wQ_j]\}}{\#\{k : Q_k \in [Q_j/w, wQ_j]\}} \geq p. \quad (\text{D5})$$

The window thus pools the neighboring runs into a local estimate of the success probability $\mathbb{P}[\delta \leq \epsilon]$ at cost Q_j . The first (smallest) accepted Q_j is taken as the convergence estimate Q^* for that run set.

To quantify uncertainty in the convergence cost, we perform bootstrap resampling of the empirical point set $\{(Q_j, \delta_j)\}$ and repeat the same window-based detection on each bootstrap replicate ($n_{\text{boot}} = 500$). This yields a bootstrap distribution of Q^* , from which we report the median and 16th/84th percentile bands.

Appendix E: Analytical Importance Sampling Budget for Gaussian Benchmarks

Using the IS notation from Section II A 1, the analytical IS budget follows directly from the central limit theorem,

$$\sqrt{N} \frac{\widehat{\mathcal{Z}}_N^{\text{IS}} - \mathcal{Z}}{\sigma_{\text{IS}}} \xrightarrow{d} \mathcal{N}(0, 1), \quad (\text{E1})$$

with asymptotic standard deviation $\sigma_{\text{IS}} = \mathcal{Z}_\phi \sqrt{\text{Var}_{p_\phi}[L/\phi]}$. For a relative error threshold ϵ and success probability p , this gives

$$Q_{\text{IS}}^* \approx \left(\frac{z_{(1+p)/2} \sigma_{\text{IS}}}{\epsilon \mathcal{Z}} \right)^2, \quad (\text{E2})$$

where $z_{(1+p)/2}$ is the $(1+p)/2$ -quantile of the standard normal distribution.

For a diagonal Gaussian surrogate and target, the normalized variance factor in this expression has a fully closed form in terms of relative shifts and width ratios. Let

$$\Delta_i := \frac{\mu_{L,i} - \mu_{\phi,i}}{\sigma_{L,i}}, \quad \tau_i := \frac{\sigma_{\phi,i}}{\sigma_{L,i}}. \quad (\text{E3})$$

A direct Gaussian integral gives

$$\frac{\mathcal{Z}_\phi^2 \text{Var}_{p_\phi}[L/\phi]}{\mathcal{Z}^2} = \prod_{i=1}^d \frac{\tau_i^2}{\sqrt{2\tau_i^2 - 1}} \exp\left(\frac{\Delta_i^2}{2\tau_i^2 - 1}\right) - 1. \quad (\text{E4})$$

This is finite if and only if $\tau_i^2 > 1/2$ in every dimension, for each $i = 1, \dots, d$.

Shift family ($\tau_i = 1, \Delta_i \neq 0$): Setting $\tau_i = 1$ gives

$$\frac{\mathcal{Z}_\phi^2 \text{Var}_{p_\phi}[L/\phi]}{\mathcal{Z}^2} = \exp\left(\sum_{i=1}^d \Delta_i^2\right) - 1. \quad (\text{E5})$$

This grows exponentially in the squared shift, explaining the catastrophic degradation of IS under mean mismatch.

Anisotropy family ($\Delta_i = 0$): Setting $\Delta_i = 0$ removes the exponential factor, giving

$$\frac{\mathcal{Z}_\phi^2 \text{Var}_{p_\phi}[L/\phi]}{\mathcal{Z}^2} = \prod_{i=1}^d \frac{\tau_i^2}{\sqrt{2\tau_i^2 - 1}} - 1, \quad (\text{E6})$$

which is finite only when $\tau_i^2 > 1/2$ for each $i = 1, \dots, d$. In the main-text anisotropy parameterization, the binding constraint comes from the stretched half, for which $\tau_i = 1/a$; finite variance therefore requires $a < \sqrt{2}$. The compressed half ($\tau_i = a$) satisfies the condition for all $a \geq 1$. At $a = \sqrt{2}$, the normalized variance diverges and $Q_{\text{IS}}^* \rightarrow \infty$.

REFERENCES

- ¹A. Gelman, J. Hwang, and A. Vehtari, "Understanding predictive information criteria for bayesian models," [Statistics and Computing](#) **24**, 997–1016 (2014).
- ²P. Goggans, R. W. Henderson, and N. Xiang, "Using nested sampling with galilean monte carlo for model comparison problems in acoustics," [Proceedings of Meetings on Acoustics](#) **19**, 055089 (2013).
- ³C. Andrieu, N. de Freitas, A. Doucet, and M. I. Jordan, "An introduction to MCMC for machine learning," [Machine Learning](#) **50**, 5–43 (2003).
- ⁴T. Jasa and N. Xiang, "Nested sampling applied in bayesian room-acoustics decay analysis," [The Journal of the Acoustical Society of America](#) **132**, 3251–3262 (2012).
- ⁵J. Veitch, V. Raymond, B. Farr, W. Farr, P. Graff, S. Vitale, et al., "Parameter estimation for compact binaries with ground-based gravitational-wave observations using the lalinference software library," [Phys. Rev. D](#) **91**, 042003 (2015).
- ⁶B. P. Abbott et al. (LIGO Scientific Collaboration and Virgo Collaboration), "Properties of the binary neutron star merger gw170817," [Phys. Rev. X](#) **9**, 011001 (2019).
- ⁷H. N. Najm, "Uncertainty quantification and polynomial chaos techniques in computational fluid dynamics," [Annual Review of Fluid Mechanics](#) **41**, 35–52 (2009).
- ⁸Y. Qian, C. Jackson, F. Giorgi, B. Booth, Q. Duan, C. Forest, et al., "Uncertainty quantification in climate modeling and projection," [Bulletin of the American Meteorological Society](#) **97**, 821 – 824 (2016).
- ⁹L. B. Pártay, A. P. Bartók, and G. Csányi, "Nested sampling for materials: The case of hard spheres," [Physical Review E](#) **89**, 022302 (2014).
- ¹⁰L. B. Pártay, G. Csányi, and N. Bernstein, "Nested sampling for materials," [The European Physical Journal B](#) **94**, 159 (2021).
- ¹¹B. Szekeres, L. B. Pártay, and E. Mátyus, "Direct computation of the quantum partition function by path-integral nested sampling," [Journal of Chemical Theory and Computation](#) **14**, 4353–4361 (2018).
- ¹²C. W. Binder, J. K. Krondorfer, and A. W. Hauser, "The ridge integration method and its application to molecular sieving, demonstrated for gas purification via graphdiyne membranes," [Mol. Syst. Des. Eng.](#) **7**, 1622–1638 (2022).
- ¹³P. G. Bolhuis and G. Csányi, "Nested transition path sampling," [Phys. Rev. Lett.](#) **120**, 250601 (2018).
- ¹⁴G. P. Lepage, "A new algorithm for adaptive multidimensional integration," [Journal of Computational Physics](#) **27**, 192–203 (1978).
- ¹⁵W. H. Press and G. R. Farrar, "Recursive stratified sampling for multidimensional monte carlo integration," [Comput. Phys.](#) **4**, 190–195 (1990).
- ¹⁶R. E. Caflisch, "Monte carlo and quasi-monte carlo methods," [Acta Numerica](#) **7**, 1–49 (1998).
- ¹⁷G. P. Lepage, "Adaptive multidimensional integration: VEGAS enhanced," [Journal](#)

- of *Computational Physics* **439**, 110386 (2021).
- ¹⁸J. Skilling, “Nested sampling,” *AIP Conference Proceedings* **735**, 395–405 (2004).
- ¹⁹J. Skilling, “Nested sampling for general Bayesian computation,” *Bayesian Analysis* **1**, 833 – 859 (2006).
- ²⁰D. Lu and D. Ricciuto, “Efficient surrogate modeling methods for large-scale earth system models based on machine-learning techniques,” *Geoscientific Model Development* **12**, 1791–1807 (2019).
- ²¹J. K. Krondorfer, C. W. Binder, and A. W. Hauser, “Symmetry- and gradient-enhanced gaussian process regression for the active learning of potential energy surfaces in porous materials,” *The Journal of Chemical Physics* **159**, 014115 (2023).
- ²²D. P. Kovács, J. H. Moore, N. J. Browning, I. Batatia, J. T. Horton, Y. Pu, *et al.*, “Maceoff: Short-range transferable machine learning force fields for organic molecules,” *Journal of the American Chemical Society* **147**, 17598–17611 (2025).
- ²³E. Uteva, R. S. Graham, R. D. Wilkinson, and R. J. Wheatley, “Active learning in gaussian process interpolation of potential energy surfaces,” *The Journal of Chemical Physics* **149**, 174114 (2018).
- ²⁴F. Lu, L. Cheng, R. J. DiRisio, J. M. Finney, M. A. Boyer, P. Moonkaen, *et al.*, “Fast near ab initio potential energy surfaces using machine learning,” *The Journal of Physical Chemistry A* **126**, 4013–4024 (2022), pMID: 35715227.
- ²⁵R. Salomone, L. F. South, C. Drovandi, D. P. Kroese, and A. M. Johansen, “Unbiased and consistent nested sampling via sequential monte carlo,” *Journal of the Royal Statistical Society Series B: Statistical Methodology* **87**, 1221–1238 (2025).
- ²⁶A. G. Wills and T. B. Schön, “Sequential monte carlo: A unified review,” *Annual Review of Control, Robotics, and Autonomous Systems* **6**, 159–182 (2023).
- ²⁷B. Peherstorfer, K. Willcox, and M. Gunzburger, “Optimal model management for multifidelity monte carlo estimation,” *SIAM Journal on Scientific Computing* **38**, A3163–A3194 (2016).
- ²⁸B. Peherstorfer, K. Willcox, and M. Gunzburger, “Survey of multifidelity methods in uncertainty propagation, inference, and optimization,” *SIAM Review* **60**, 550–591 (2018).
- ²⁹M. B. Giles, “Multilevel monte carlo methods,” *Acta Numerica* **24**, 259–328 (2015).
- ³⁰S. T. Tokdar and R. E. Kass, “Importance sampling: a review,” *WIREs Computational Statistics* **2**, 54–60 (2010).
- ³¹G. Ashton, N. Bernstein, J. Buchner, X. Chen, G. Csányi, A. Fowlie, *et al.*, “Nested sampling for physical scientists,” *Nature Reviews Methods Primers* **2**, 39 (2022).
- ³²F. Feroz, M. Hobson, and M. Bridges, “Multinest: an efficient and robust bayesian inference tool for cosmology and particle physics,” *Monthly Notices of the Royal Astronomical Society* **398**, 1601–1614 (2009).
- ³³E. Higson, W. Handley, M. Hobson, and A. Lasenby, “Dynamic nested sampling: an improved algorithm for parameter estimation and evidence calculation,” *Statistics*

- and Computing **29**, 891–913 (2019).
- ³⁴J. S. Speagle, “dynesty: a dynamic nested sampling package for estimating bayesian posteriors and evidences,” *Monthly Notices of the Royal Astronomical Society* **493**, 3132–3158 (2020).
- ³⁵W. J. Handley, M. P. Hobson, and A. N. Lasenby, “POLYCHORD: next-generation nested sampling,” *Monthly Notices of the Royal Astronomical Society* **453**, 4384–4398 (2015).
- ³⁶J. Buchner, “Nested sampling methods,” *Statistics Surveys* **17**, 169 – 215 (2023).
- ³⁷J. Buchner, “UltraNest – a robust, general purpose Bayesian inference engine,” *Journal of Open Source Software* **6**, 3001 (2021).
- ³⁸R. M. Neal, “Slice sampling,” *The Annals of Statistics* **31**, 705–767 (2003).
- ³⁹W. von der Linden, V. Dose, and U. von Toussaint, *Bayesian Probability Theory: Applications in the Physical Sciences* (Cambridge University Press, Cambridge, 2014).
- ⁴⁰A. Fowlie, W. Handley, and L. Su, “Nested sampling with plateaus,” *Monthly Notices of the Royal Astronomical Society* **503**, 1199–1205 (2021).
- ⁴¹D. Schittenhelm and P. Wacker, “Nested sampling and likelihood plateaus,” (2021), [arXiv:2005.08602 \[math.ST\]](https://arxiv.org/abs/2005.08602).
- ⁴²C. R. Keeton, “On statistical uncertainty in nested sampling,” *Monthly Notices of the Royal Astronomical Society* **414**, 1418–1426 (2011).
- ⁴³C. Walter, “Point process-based monte carlo estimation,” *Statistics and Computing* **27**, 219–236 (2017).
- ⁴⁴E. Higson, W. Handley, M. Hobson, and A. Lasenby, “Sampling Errors in Nested Sampling Parameter Estimation,” *Bayesian Analysis* **13**, 873 – 896 (2018).
- ⁴⁵N. Chopin and C. P. Robert, “Properties of nested sampling,” *Biometrika* **97**, 741–755 (2010).
- ⁴⁶J. Skilling, “Nested sampling’s convergence,” *AIP Conference Proceedings* **1193**, 277–291 (2009).
- ⁴⁷E. Cameron and A. Pettitt, “Recursive pathways to marginal likelihood estimation with prior-sensitivity analysis,” *Statistical Science* **29**, 397–419 (2014).
- ⁴⁸F. Feroz, M. P. Hobson, E. Cameron, and A. N. Pettitt, “Importance nested sampling and the multinest algorithm,” *The Open Journal of Astrophysics* **2**, 10 (2019).